NASA CONTRACTOR REPORT

NASA CR-674

NASA CR-674



# A "CRITICAL" TRACKING TASK FOR MAN-MACHINE RESEARCH RELATED TO THE OPERATOR'S EFFECTIVE DELAY TIME

## PART II. EXPERIMENTAL EFFECTS OF SYSTEM INPUT SPECTRA, CONTROL STICK STIFFNESS, AND CONTROLLED ELEMENT ORDER

*by J. D. McDonnell and H. R. Jex*

*Prepared by*
SYSTEMS TECHNOLOGY, INC.
Hawthorne, Calif.
*for Ames Research Center*



NATIONAL AERONAUTICS AND SPACE ADMINISTRATION • WASHINGTON, D. C. • JANUARY 1967

NASA CR-674

# A "CRITICAL" TRACKING TASK FOR MAN-MACHINE RESEARCH RELATED TO THE OPERATOR'S EFFECTIVE DELAY TIME

## PART II. EXPERIMENTAL EFFECTS OF SYSTEM INPUT SPECTRA, CONTROL STICK STIFFNESS, AND CONTROLLED ELEMENT ORDER

By J. D. McDonnell and H. R. Jex



Prepared under Contract No. NAS 2-2288 by
SYSTEMS TECHNOLOGY, INC.
Hawthorne, Calif.

for Ames Research Center

NATIONAL AERONAUTICS AND SPACE ADMINISTRATION

For sale by the Clearinghouse for Federal Scientific and Technical Information
Springfield, Virginia 22151 – Price $2.50

## FOREWORD

This report was prepared under Contract NAS2-2288 between Systems Technology, Inc., Hawthorne, California, and the National Aeronautics and Space Administration. The NASA project monitor was George Rathert. The STI technical director was Duane T. McRuer, and the project engineer for the second phase of this contract was John D. McDonnell.

The experiments were carried out at the Franklin Institute Laboratories for Research and Development, Philadelphia, Pennsylvania, with the help of William C. Reisener, Jr. The authors gratefully acknowledge the help with calculations from Anil V. Phatak, and the equipment support given by Keith A. Ferrick.

## ABSTRACT

The Critical Task, previously described in Part I of this report, consists of a closed-loop tracking task in which an increasingly unstable controlled element is used to yield a measure of the operator's effective time delay while tracking. In this part of the report, the task has been further developed through the analysis of additional data.

In a series of experiments, it was found that the human operator's characteristics do not change as the system input level is decreased; hence, the critical task yields a valid limit when excited solely by the operator's remnant. The effects on the operator of different control stick types (force, spring, and free) are investigated, and the differences in critical task scores are related to the operator's describing function characteristics. Step reaction time data are compared with the continuous measures of effective time delay and the autopacer scores. A sample analysis to determine the number of autopacer trials necessary to achieve a confident measure is made. Finally, data are presented for a second-order critical task in which an integrator precedes the first-order divergence.

CONTENTS

## FIGURES

## SYMBOLS

| | |
|---|---|
| $c(t)$ | Operator output time function, limb position |
| $C(j\omega)$ | Fourier transform of operator output |
| $e(t)$ | Error time function |
| $E(j\omega)$ | Fourier transform of error |
| $G$ | Total open-loop describing function, $Y_p Y_c$ |
| $i(t)$ | Forcing function time function |
| $I(j\omega)$ | Fourier transform of forcing function |
| $j\omega$ | Imaginary part of the complex variable, $s = \sigma \pm j\omega$ |
| $K$ | Open-loop gain |
| $K_c$ | Controlled element gain |
| $K_p$ | Human operator static gain |
| $m(t)$ | System output time function |
| $M(j\omega)$ | Fourier transform of system output |
| $\overline{n^2}$ | Mean-squared remnant, $\frac{1}{2\pi}\int_0^\infty \Phi_{nn} d\omega$ |
| $N$ | Number of subjects |
| $N_c(j\omega)$ | Fourier transform of operator remnant |
| $RT$ | Reaction time |
| $s$ | Complex variable, $s = \sigma \pm j\omega$; Laplace transform variable |
| $t$ | Time |
| $T$ | Time constant |
| $T_c$ | Critical or limiting time constant as obtained from the autopacer, $T_c = 1/\lambda_c$ |
| $T_I$ | General lag time constant of human pilot describing function |
| $T_K$, $T_K'$ | Low frequency lead and lag kinesthetic time constants in precision model of human pilot describing function |

| | |
|---|---|
| $T_L$ | General lead time constant of human pilot describing function |
| $T_N$ | First-order lag time constant approximation of the neuromuscular system |
| $T_{N_1}$ | First-order lag time constant of the neuromuscular system |
| $T_R$ | Run length |
| $Y$ | Transfer function |
| $Y_c(s)$ | Controlled element (machine and display) transfer function |
| $Y_{CL}$ | Closed-loop transfer function |
| $Y_{OL}$ | Open-loop transfer function |
| $Y_p$ | Pilot describing function |
| $\alpha$ | Low frequency phase approximation parameter, $\alpha = 1/T_K - 1/T_K'$ |
| $\zeta$ | Damping ratio |
| $\zeta_{CL}$ | Closed-loop damping ratio |
| $\zeta_N$ | Damping ratio of second-order component of the neuromuscular system |
| $\rho_a$ | Relative remnant at pilot's output, $\sqrt{1 - \overline{n^2}/\overline{c^2}}$ |
| $\sigma$ | Standard deviation, real part of complex variable, $s = \sigma \pm j\omega$ |
| $\sigma_i$ | RMS value of the forcing function |
| $\lambda$ | Value of unstable root of first-order critical task |
| $\lambda_c$ | Critical or limiting root value as obtained from the autopacer, $\lambda_c = 1/T_c$ |
| $\tau$ | Pure time delay |
| $\Delta\tau$ | Incremental time delay |
| $\tau_d$ | Physiological time delay |
| $\tau_e$ | Effective time delay |
| $\tau_r(t)$ | Time-varying time delay, source of operator remnant |
| $\varphi$ | Phase angle |
| $\Delta\varphi$ | Incremental phase angle |

| | |
|---|---|
| $\varphi_M$ | Phase margin |
| $\Phi_{cc}(\omega)$ | Pilot's output power spectral density |
| $\Phi_{ee}(\omega)$ | Error power spectral density |
| $\Phi_{ec}$ | Cross power spectral density between e and c |
| $\Phi_{ic}$ | Cross power spectral density between i and c |
| $\Phi_{ie}$ | Cross power spectral density between i and e |
| $\Phi_{ii}$ | Forcing function power spectral density |
| $\Phi_{mm}$ | System output power spectral density |
| $\Phi_{nn}$ | Closed-loop remnant spectral density, at pilot's output |
| $\Phi_{nn_c}$ | Open-loop remnant spectral density, at pilot's output, $\lvert 1 + Y_p Y_c \rvert^2 \Phi_{nn}$ |
| $\omega$ | Angular frequency, rad/sec |
| $\omega_c$ | System crossover frequency, i.e., frequency at which $\lvert Y_p Y_c \rvert = 1$ |
| $\omega_{CL}$ | A closed-loop inverse time constant or frequency |
| $\omega_i$ | Forcing function bandwidth |
| $\omega_N$ | Undamped natural frequency of second-order part of the neuromuscular system |
| $\omega_u$ | Crossover frequency for neutral stability |
| $\doteq$ | Approximately equal to |
| $\angle$ | Angle of |
| dB | Decibels; $20 \log_{10}$ ( ) if an amplitude quantity, e.g., $\lvert Y_p \rvert$ |
| $\lvert\ \rvert$ | Magnitude |
| $\lvert\ \rvert_{dB}$ | Magnitude in dB |
| $\bar{(\ )}$ | Mean value |

# SECTION I

# INTRODUCTION

A closed-loop compensatory tracking has been developed which uses an increasingly unstable controlled element to yield a measure of the operator's effective delay time while tracking. The main body of data and the theoretical analysis of the task is reported in Part I of this report (ref. 1). The experimental program for this research was undertaken in February 1965 at the Franklin Institute where, as part of the over-all experimental plan, some data were obtained which were rather incidental to the main program but which could not be obtained economically at a later date. It is these data that are reported herein, with the purpose in mind of further advancing the critical task theory, understanding the observed behavior of the operator, and validating some of the theories which have been evolved. It is assumed throughout this report that the reader is completely familiar with the companion Part I report (ref. 1), so that some details are not repeated here.

The data obtained cover several areas of interest. Each area is essentially independent, hence this report has been written in the form of a collection of experiments. Section II covers the effects of varying input level on the operator to validate the use of the autopacer without an input. Section III contains the effects of different control sticks on the results. Section IV presents concurrently measured step reaction time data and an analysis of trial size, while Part V covers some preliminary second-order critical task data.

## SECTION II

## INPUT EFFECTS ON OPERATOR CHARACTERISTICS

### A. GENERAL

When the controlled element of a manual control system is unstable, the operator must exercise control even in the absence of an input, as would any linear controller. A mechanical or electrical controller would have no noticeable output (control would be accomplished with very small motions) while the human operator exhibits varying degrees of control action depending on the level of instability. An explanation is that the operator's remnant (sometimes attributed to "noise" injection or time variation about mean parameters, ref. 2) excites the system and is, in effect, a system input. The STI critical task, which utilizes an unstable plant, was developed not as a tracking task, per se, but as a device to measure certain operator characteristics while in closed-loop operation. Thus, if these operator characteristics could be adequately measured using only remnant for system excitation, economies in mechanization and operation would result. The experiment described below was carried out to determine the nature and assess the validity of the effective time-delay measures obtained as the input level is progressively reduced to zero.

### B. DESCRIPTION OF THE EXPERIMENT

The experiment was carried out at the Franklin Institute simultaneously with the experiments described in reference 1 and used the same simulation and analyzers to take data for describing function and remnant calculations. As will be recalled from reference 1, the system input consisted of the sum of ten sinusoids with their amplitude adjusted so that the spectrum was rectangularly shaped and had a higher frequency, lower amplitude "shelf" as shown in figure 1.

The experimental variables of the input were chosen to be the bandwidth, $\omega_I$, and the mean-square amplitude, given by

$$\sigma_i^2 = \frac{1}{2}\sum_{j=1}^{n} A_j^2 \qquad (1)$$

where $A_j$ is the peak amplitude of the jth sinusoid. Random phasing between the components gives a random-appearing input signal.

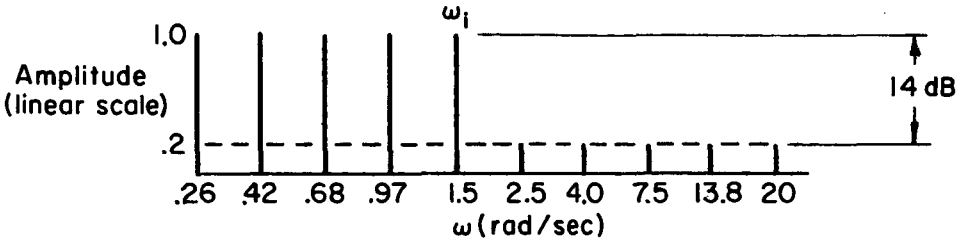


Figure 1. Input Spectrum (B6' shape, $\omega_i$ = 1.5 rad/sec)

The Measurement Systems, Inc. Model 435 force stick was used for all runs and the first-order sub-critical task of reference 1 was used with $\lambda$ = 4 rad/sec ($\lambda$ is the unstable root value). The subject was the same in all the Franklin Institute critical task runs. Approximately a dozen runs were made specifically to determine input effects. Four input levels and three input bandwidths were used, and two no-input runs were tape recorded for further power-spectral analysis by the dc analyzer.

## C. CRITERION FOR VALIDITY AND EXPERIMENTAL DESIGN

The approach for determining the validity of no-input measures is as follows.

Consider the typical manual control system shown in figure 2. In the absence of a system input, I, any attempt to measure the linear characteristics, $Y_p$, of the operator would result in

$$Y_p = \frac{C}{E} = -\frac{1}{Y_c} \qquad (2)$$

unless a specific form is assumed for $N_c$, the operator's injected noise or remnant. Let us assume for the moment that the linear description of the operator does not change in the absence of an input, i.e., that for $Y_c = 1/(-Ts + 1)$ it is given by the "extended crossover" model,

$$Y_p = K_p e^{(\alpha/s - \tau s)} \tag{3}$$

to an adequate approximation (this is shown to be an adequate model in ref. 1 when a system input is present). The characteristic equation of figure 2 is unchanged in the absence of an input so the stability criterion is unchanged. We can therefore show that a critical instability, $\lambda_c$, obtained without an input is valid if we can show that the form of $Y_p$ doesn't change when the input is progressively reduced to zero.

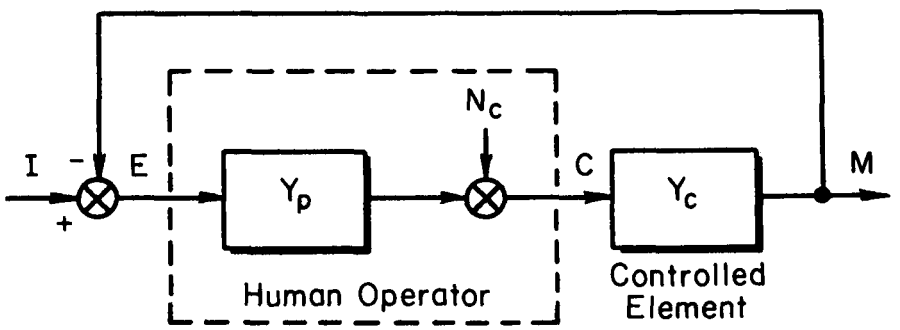


Figure 2. A Single-Loop Manual Control System

The experimental design to permit this extrapolation to zero input is as follows:

1. A series of inputs having a constant effective bandwidth but decreasing rms levels is given the operator, and the resulting describing functions, control output power spectra and remnant power spectra are measured for each. The describing functions and remnant are then extrapolated to zero input level. The extrapolated data are used to "predict" the control output power spectrum that remains when the input is removed, and this is compared with the measured control output spectrum.

2. Since the operator remnant appears to be wide-band (ref. 3), a very low amplitude input can be used while being subjectively masked, at the error display, by the relatively large remnant-excited signals present during near-critical tracking. This "subliminal" input is nevertheless acted on by the operator and permits a measurement of $Y_p$ under subjectively no-input conditions, albeit with degraded signal-to-noise ratios.

## D. DISCUSSION OF THE DATA

The data obtained from the watthour meter and dc cross-spectral analyzers (ref. 3) can be reduced to yield results of essentially four types: (1) describing functions, $Y_p(j\omega)$, (2) control output power spectra, $\Phi_{cc}(\omega)$, (3) operator's control remnant, $\varphi_{nn}(\omega)$, and (4) average performance measures, $\overline{c^2}$, $\overline{e^2}$, and $\rho_{ac}$. The first three types indicate any frequency sensitive changes occurring within the operator, while the fourth category shows how the net closed-loop performance varies. All four are useful as clues to behavior, and each will be discussed in turn below.

### 1. Describing Function Data

Operator describing functions have been computed in the manner described in reference 3 for selected runs from watthour meter analyzer data taken during the experiments. The describing functions, plotted in figure 3, are computed for three input levels. The levels were chosen on the basis of subjective operator difficulty and are considered to be representative of "small, medium, and large" inputs.

The most notable difference between input conditions apparent in figure 3 is that the low amplitude input data is scattered.* This emphasizes that the analyzer has difficulty resolving measures at a frequency where only a few cycles of the input occur in a run length.

---

*Machine problems prevented data recording at 13.8 r/s on the day the 1/16" and 1/4" rms runs were made, hence the absence of describing function points.

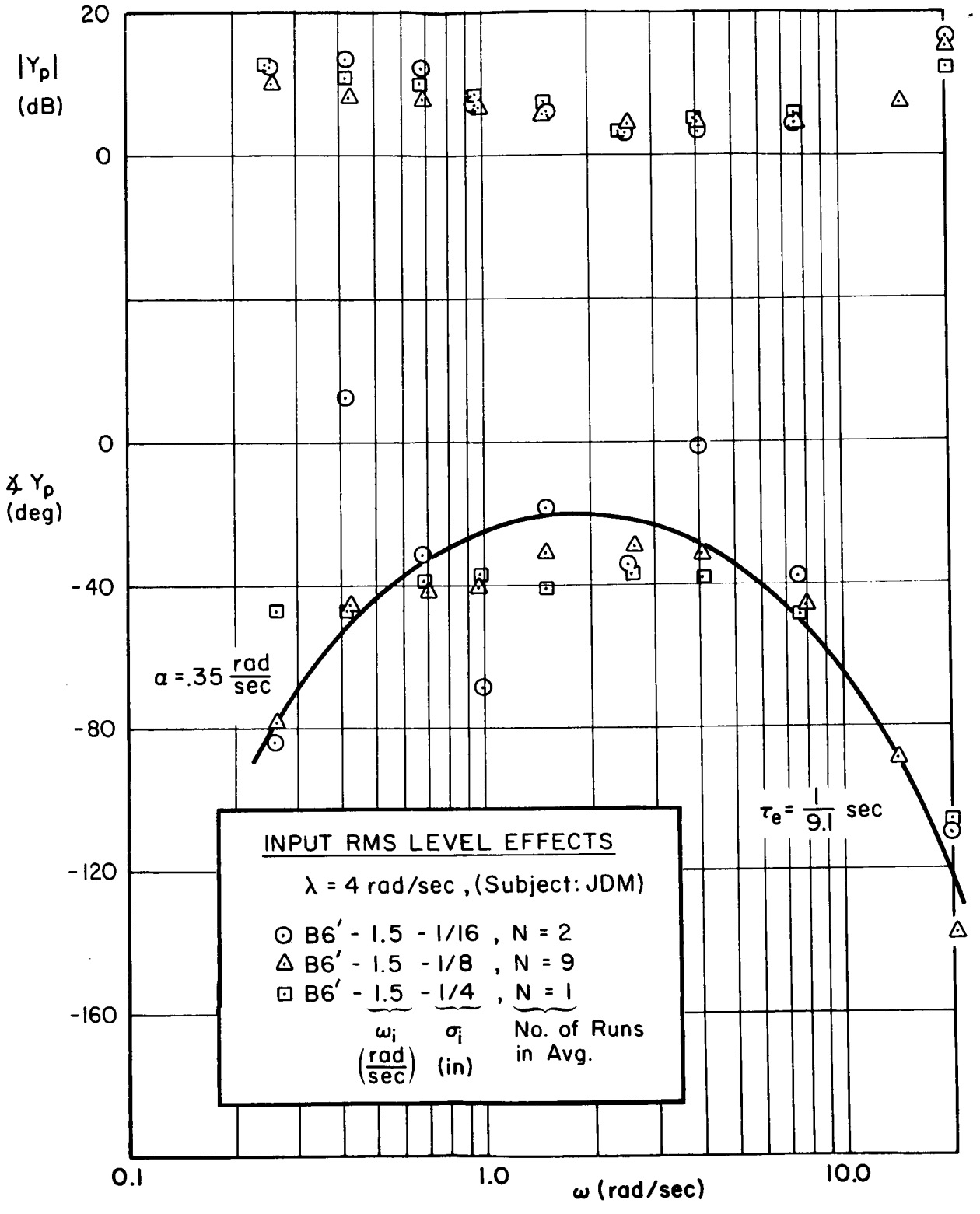


Figure 3. Describing Functions Showing Input Level Effects

The difficulty is compounded by the low signal-to-noise environment of the low amplitude input. The high frequency portion is reliable, however, and careful inspection of the high frequency portion of the describing function phase yields no trends or significant effects from input level variation. The appropriate curve fit from reference 1 ($\alpha$ = 0.35 rad/sec, $\tau_e$ = 0.110 sec) is shown in figure 3. These results are consistent with the work of Elkind (see ref. 4) where it was determined that system closed-loop characteristics remained the same as the input was diminished. The amplitude ratio data also indicates that little change occurs, but has not been discussed since it is less sensitive than the phase to system changes (note that the operator model, eq. (3), has only one parameter, $K_p$, that affects the amplitude ratio).

Additional describing function data were taken which allow a check of input effect by varying bandwidth. Figure 4 shows three bandwidth cases (shelf only, $\omega_i$ = 1.5 and 4.0 rad/sec). The extended crossover model fit is shown here also ($\alpha$ = 0.35 rad/sec, $\tau_e$ = 0.110 sec) and again no difference is noticeable in the high frequency character of the describing functions. It is interesting to note that reference 3 did obtain an effect on $\tau_{eff}$ from bandwidth variation, but there the operators were not operating as near their stability limits, and were therefore not constrained to use their minimum $\tau_{eff}$.

It is concluded, then, that at near critical instabilities, no further change occurs in the operator's describing function as the input is reduced either by decreasing the amplitude or the bandwidth.

## 2. Correlated and Remnant Power Spectra

The describing function shows the operator's linear characteristics at input frequencies, but the corresponding power levels at which he is operating (determined by closed-loop characteristics) are not obvious at all, nor can any information be obtained about his output at other than input frequencies. For these reasons, power spectra nicely supplement describing functions and have been computed for pertinent runs here. The methods and procedures used to compute spectra from both the dc and

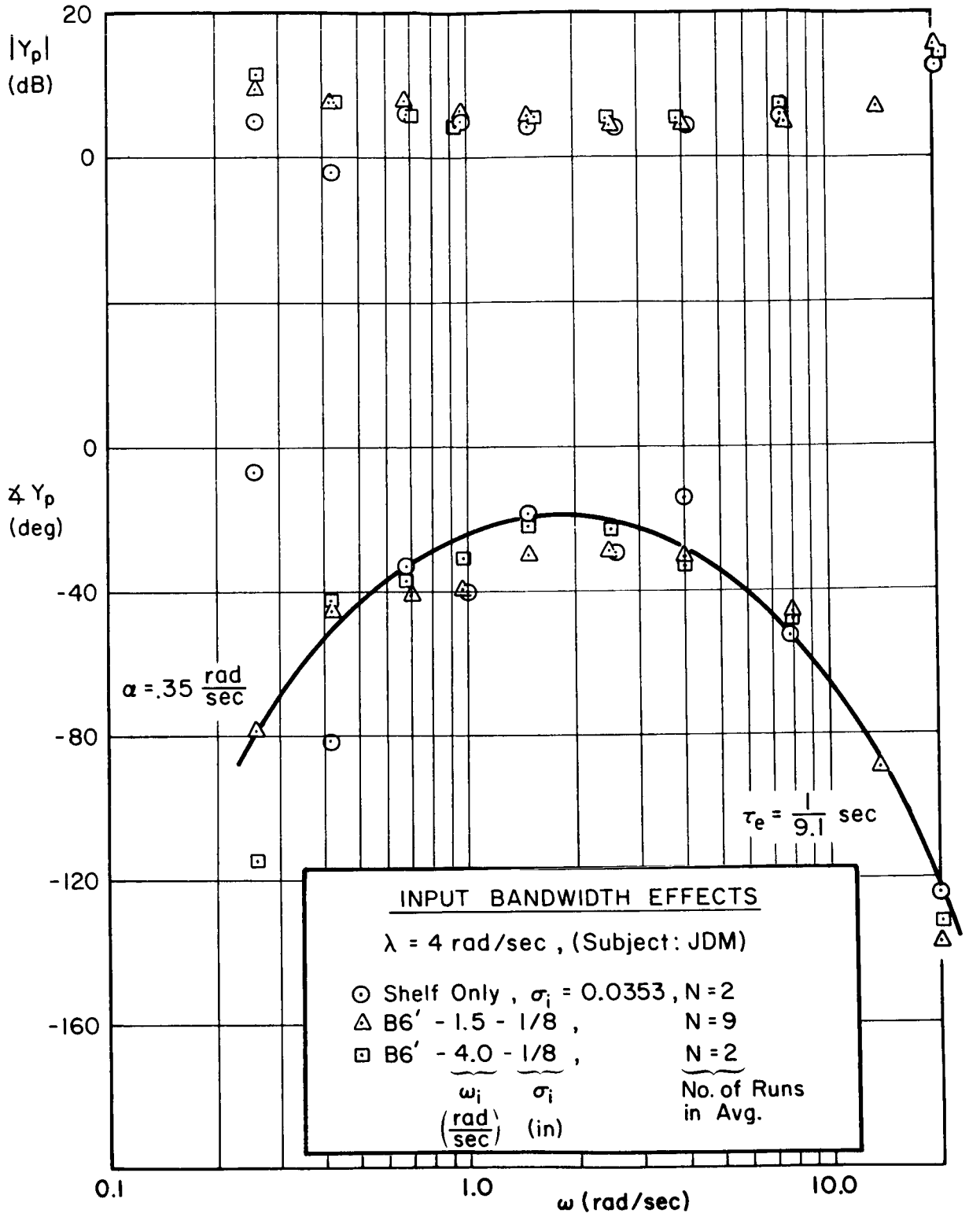


Figure 4. Describing Functions Showing Input Bandwidth Effects

watthour meter analyzers are rather lengthy and so will not be noted here (see refs. 3 and 5 for details).

Since the input is composed of a sum of sinusoids, the portion of the operator's output which is correlated with the input is also a sum of sinusoids. The power of these sinusoids is represented by the symbol, $\Phi_{cc_i}$, which is the output power, cc, correlated with the input, i. On the other hand, at frequencies between input frequencies, there is evidence that the operator generates an output over all frequencies (ref. 3). It is therefore appropriate to represent the operator's uncorrelated output (his remnant) as a density, $\Phi_{nn}$. Consider now the measurement of the power spectra at an input frequency with the dc analyzer. The analyzer has a finite bandwidth, $\Delta\omega$, so that it is not only measuring the correlated power, but the remnant within $\Delta\omega$. The power measured will thus be the sum of the power in the sinusoid ("spike" power) and the area under the curve in sketch A. The techniques for separating

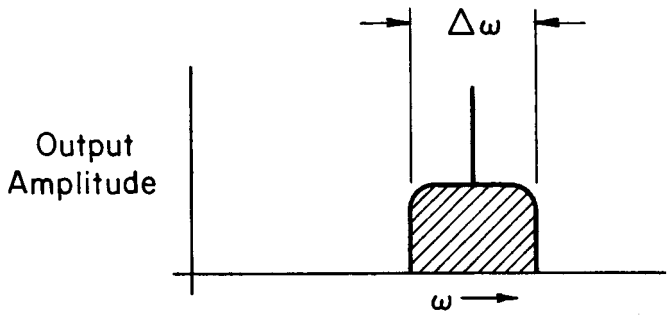


Sketch A. Measurement Bandwidth of the DCA

this resultant measure into $\Phi_{cc_i}$ (the squared amplitude of the "spike") and $\Phi_{nn}$ (the amplitude of the crosshatched area of the curve) are contained elsewhere (ref. 3), but now the reader will not be perplexed at finding remnant at input frequencies in some of the following figures.

Before proceeding with the data presentation, it is interesting to compare the results of the two possible measurement methods. Figure 5 presents the average power spectra for 5 runs obtained from the watthour

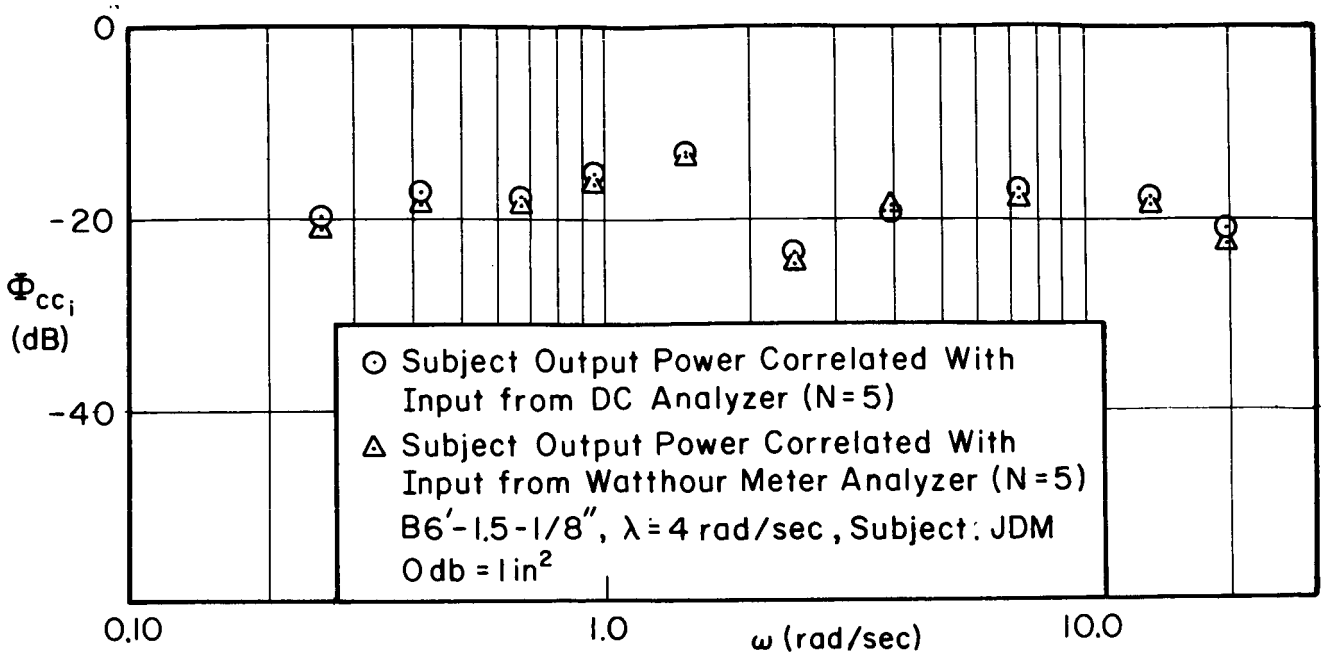


Figure 5. Comparison of DC Analyzer and Watthour Meter Analyzer Data

meter analyzer and the dc analyzer (the same 5 runs were used for each). There it is apparent that the agreement is excellent between the independent and entirely different techniques.

The three conditions of interest are: (1) the base condition with the B6' – 1.5 – 1/8" input, (2) the shelf input condition, $\sigma_i$ = 0.035", and (3) no input at all. Figures 6 and 7 show the measured correlated power, $\Phi_{cc_i}$, for the base condition and the shelf input condition, respectively. The solid line in each figure is the theoretical spectra obtained from

$$\Phi_{cc_i} = \left| \frac{Y_p}{1 + Y_p Y_c} \right|^2 \Phi_{ii} = Y_p^2 G_{ie}^2 \Phi_{ii} \qquad (4)$$

where the extended crossover model (see fig. 4, ref. 1) is used for $Y_p$.

A comparison of figures 6 and 7 shows that even though the low frequency portions of the two are different by 14 dB, the operator's linear description remains unchanged, as evidenced by the agreement between the data points and the solid lines.

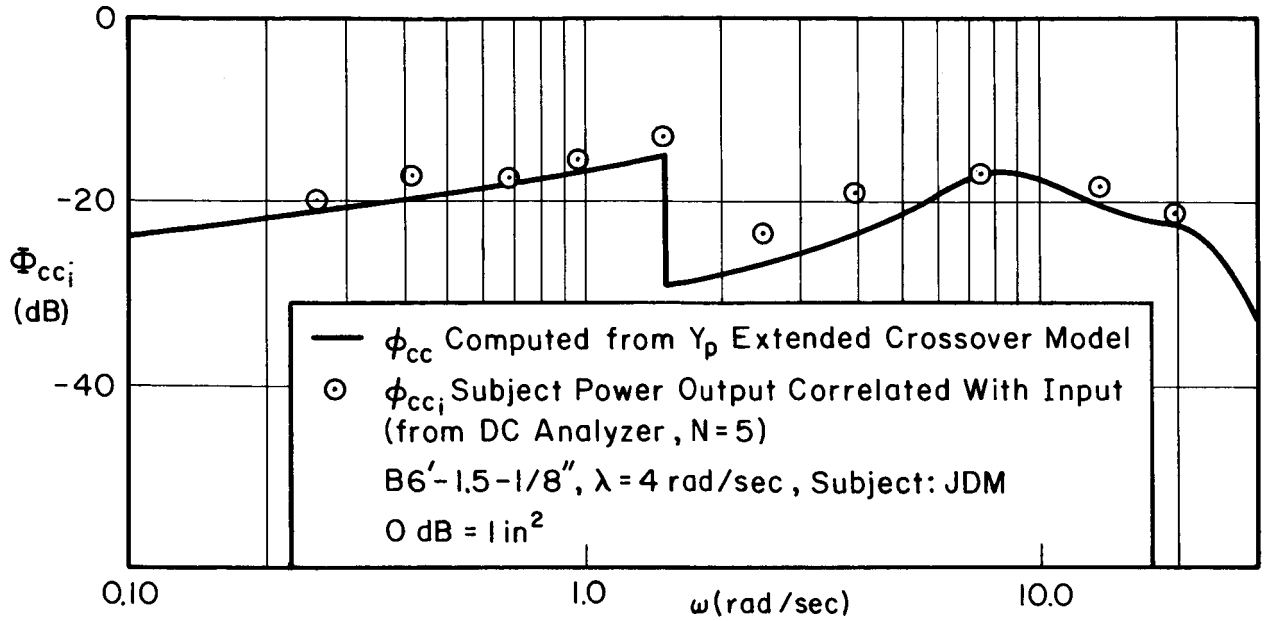


Figure 6. Comparison of Base Run Power Spectra with the Model

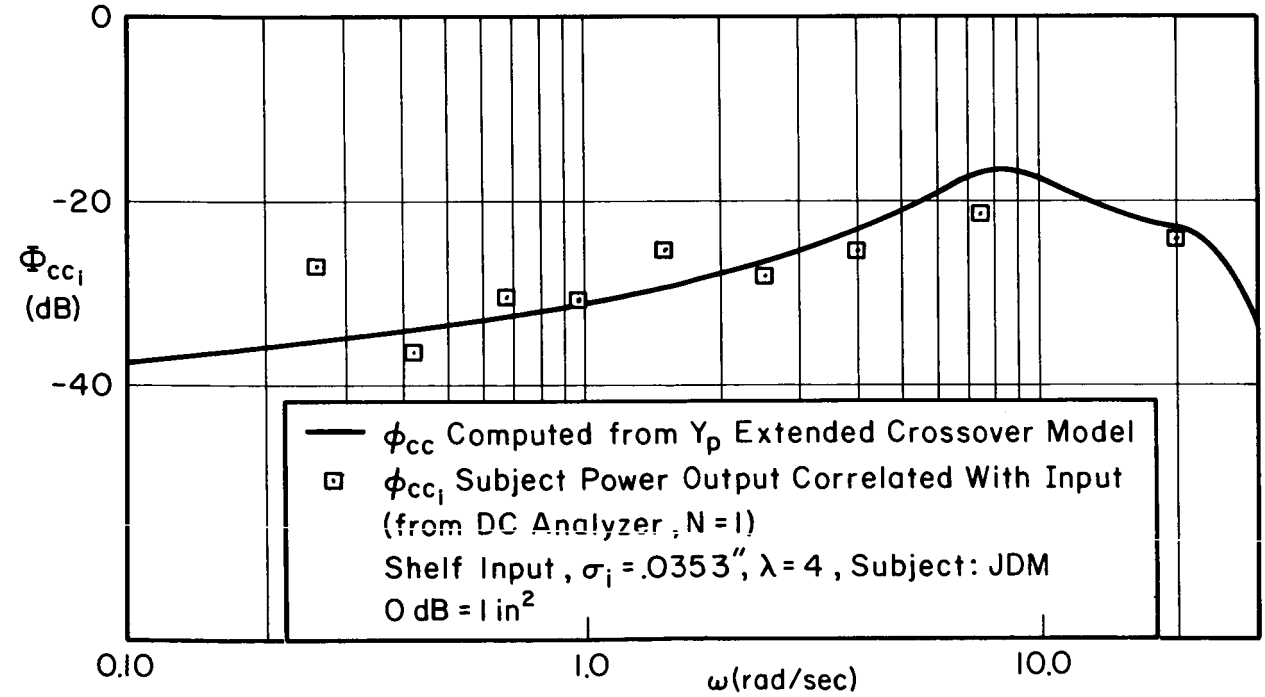


Figure 7. Comparison of Shelf Input Power Spectra with the Model

It is also interesting to note that the shelf portion of the input is barely detectable by the operator, and yet the power he expends over these frequencies ($2 < \omega < 20$ rad/sec) is considerable.

The above data indicates that the operator doesn't change his form as the input is decreased. We can get a further indication of his behavior by measuring power output when no input is present. In such a case, his entire output is remnant, and it can be compared with the remnant present in the input cases. Figure 8 shows such a comparison. Measures were made at input frequencies as well as each half-rad/sec between 3 and 10 rad/sec.

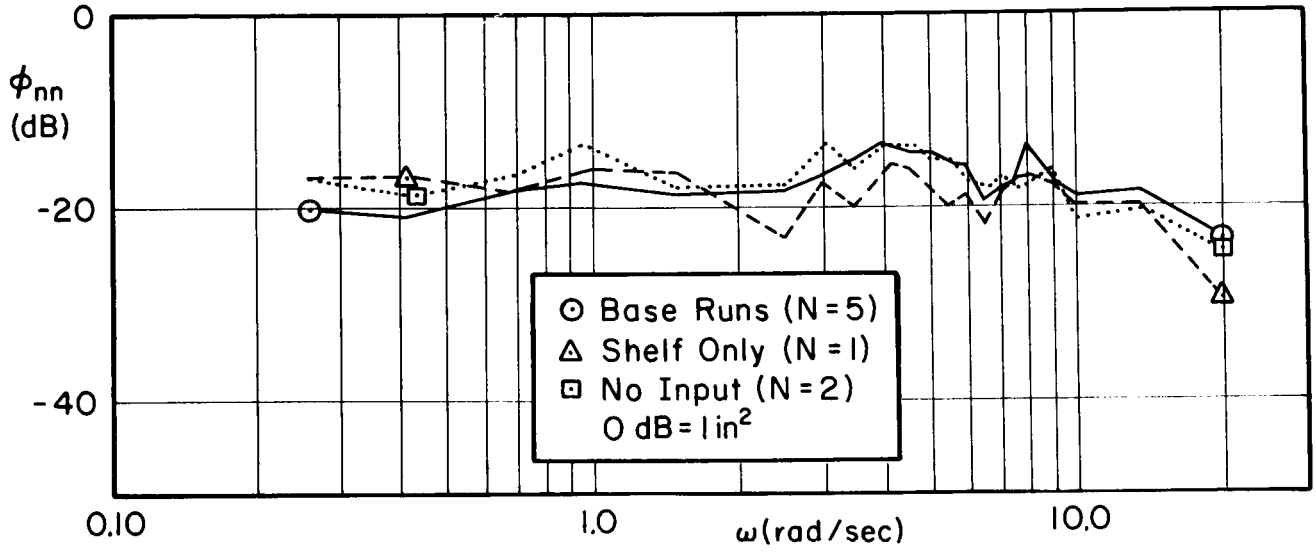


Figure 8. Comparison of Remnant Power Spectral Density for Base Runs, Shelf Input, and No-Input Cases

It is apparent from the figure that the remnant doesn't vary appreciably as the input is varied from none at all to one of considerable size.

### 3. Average Measures

The watthour meter analyzer affords average measures of subject output (both correlated and uncorrelated) with relative ease. Thus measures are available which provide a crosscheck on the power spectra and which are a

good indication of over-all behavior and performance. The most enlightening of these measures are the operator's total rms output and his uncorrelated rms output (fig. 9). As is the case with the power spectra, the total output increases with input level, while the remnant remains of the same order of magnitude. In fact, it would probably be safe to say that the rms remnant is essentially constant.

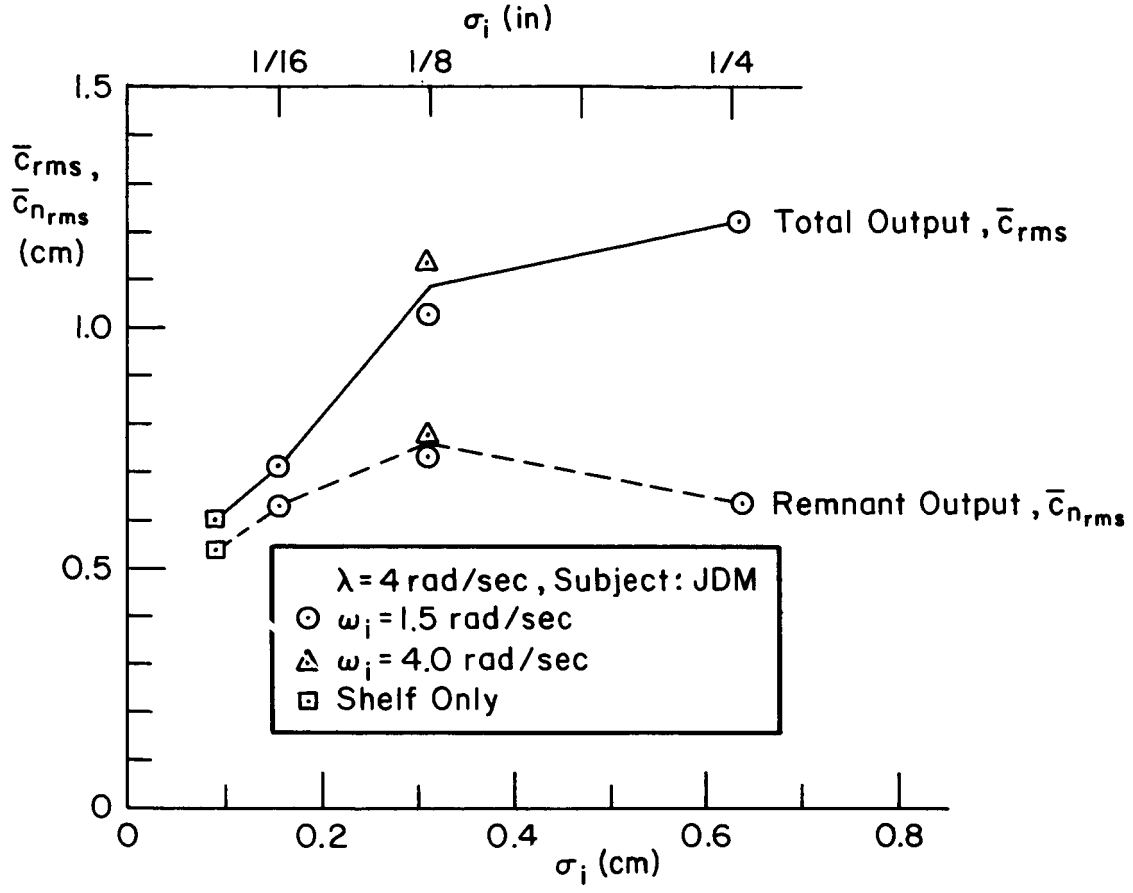


Figure 9. Total and Remnant Average Output Variation With Input Level

The relative remnant is defined as

$$\rho_a^2 = 1 - \frac{\overline{c_n^2}}{\overline{c^2}} = \frac{\overline{c_i^2}}{\overline{c_i^2} + \overline{c_n^2}} \qquad (5)$$

and is plotted in figure 10 from watthour meter data. The theoretical $\rho_a$ could be computed from equation (5), assuming that the remnant $c_n$ is constant, and compared with the experimentally obtained values in figure 10, but it is felt that the data are too sparse at this time. The conclusion, however, that the operator's remnant is a fairly constant part of his output is evident.

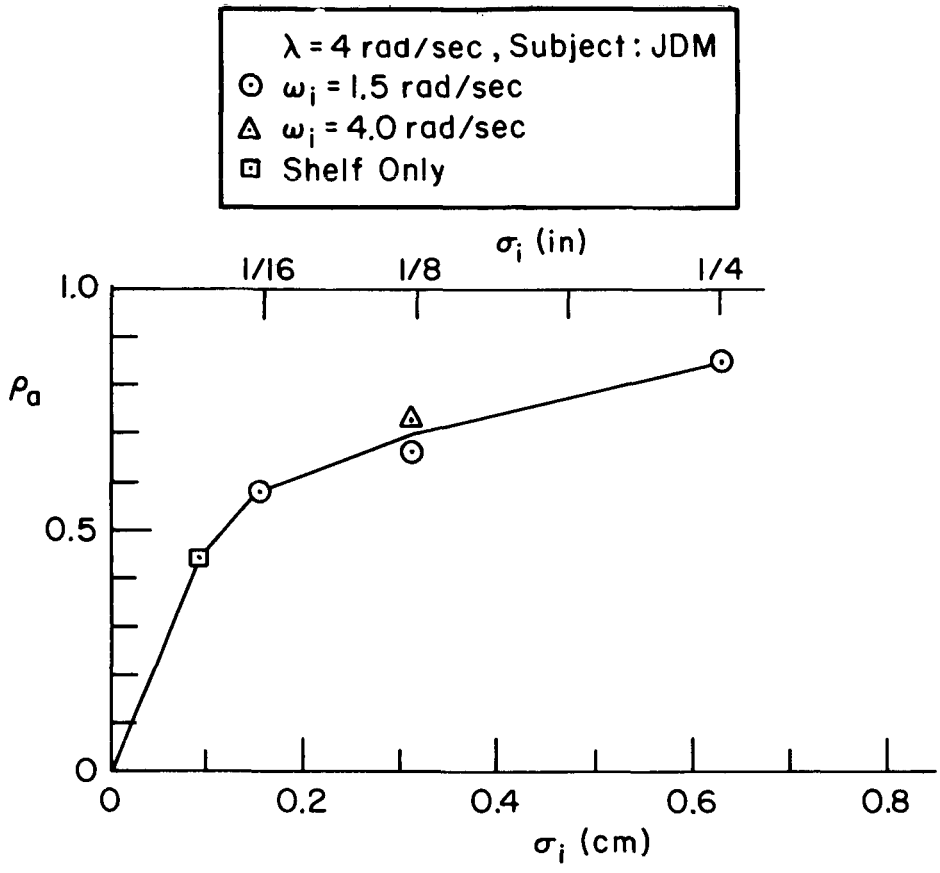


Figure 10. Relative Remnant Variation with Input Level

## E. AUTOPACER ASSESSMENT

It is apparent from the discussion to this point that the operator retains his form of behavior in the absence of an input. But a difference in autopacer critical instability scores obtained with and without an input has been observed, so what is the cause of the difference? The answer was given in references 1, 6, and 7. In reference 1 it was noted that as the system approaches instability, the ratio of error to input

grows until, at neutral stability, the error is infinite. A typical error performance curve is sketched in figure 11 for a system where some optimum strategy, such as maximum gain margin, is being used. There, for a given input, the resultant $\lambda_c$ is the value obtained when the error reaches the display limits. Now, if the input size is increased, the "scope limit" line on the figure would effectively be moved down, hence $\lambda_c$ would decrease. The ideal is to have the display limit very much greater than the rms input or effective remnant.

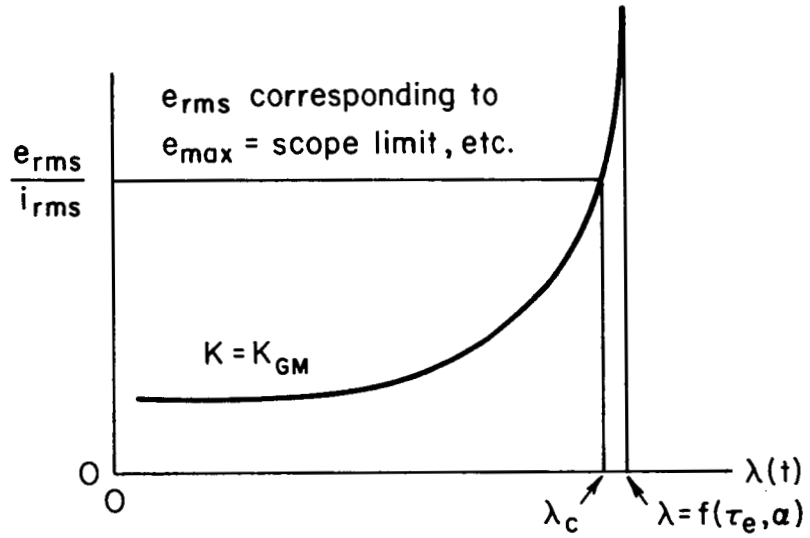


Figure 11. Characteristic Error Performance for Critical Task

This phenomenon was checked by mechanizing an analog subject on the computer and then varying the input level. The results, documented in reference 6, are shown in figure 12. Note that for zero input the resulting critical time constant is equal to the delay set in on the analog pilot. As the input increases, so does the critical time constant, i.e., $\lambda_c$ $(= 1/T_c)$ decreases. This curve, which is supported by a theoretical analysis based on input amplitude probability distributions in reference 7, is not intended as a calibration of any sort, since such factors as input frequency content, the terminal autopacer rates, operator remnant levels, etc., all can slightly influence the resulting scores. It does show, however, that the minimum input yields the score most nearly equal to the desired critical limit.

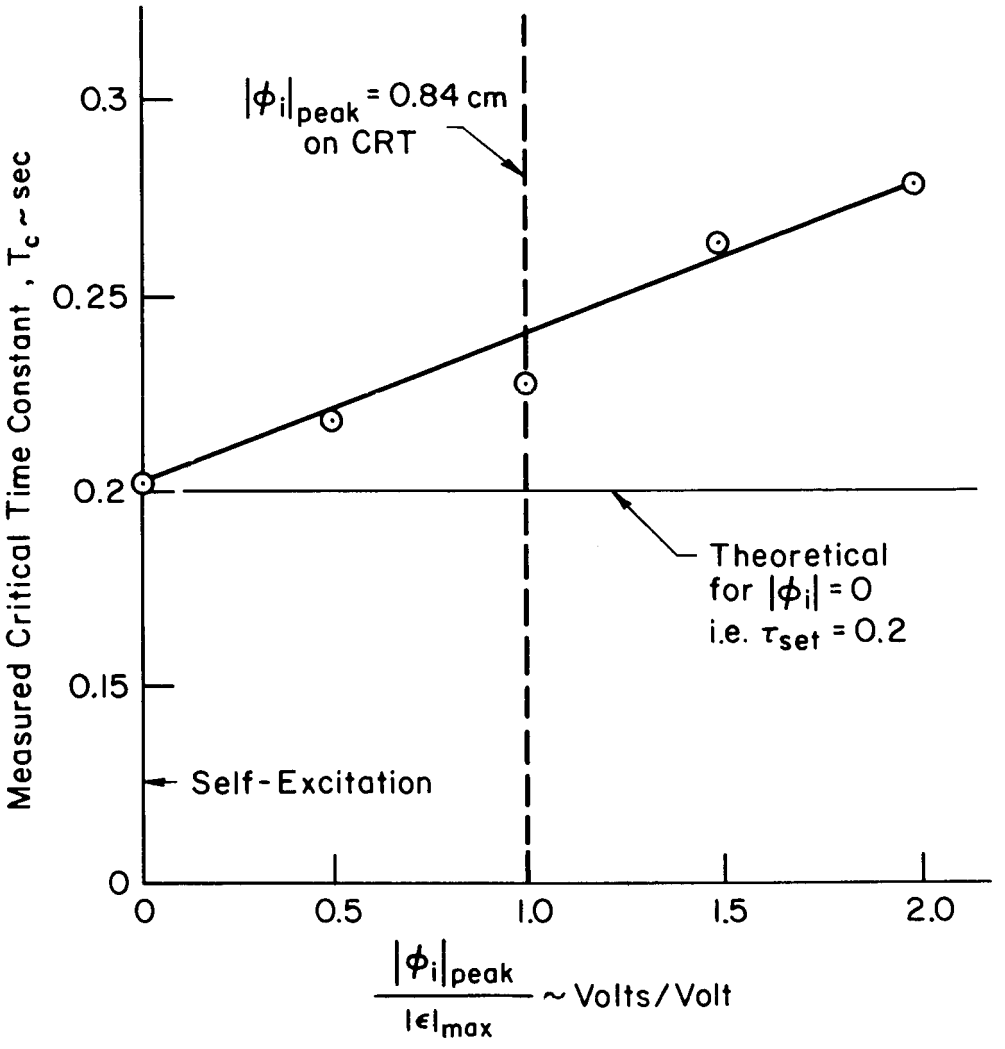


Figure 12. Effect of Random Input on Measured $T_c$ Using a Known and Fixed Value "$\tau_{set}$"

## F. SUMMARY AND CONCLUSIONS

The effects of an input on the operator under near-critical conditions can be summarized as follows:

- The operator's describing function is pushed to a limit and shows no further change with input amplitude or bandwidth.
- The operator's output power spectra show that the part of his output correlated with the input decreases with input level as predicted with the model.
- The power and spectral shape of the operator's output remnant remains essentially unchanged by input level.

It can therefore be concluded that near the critical task limits the operator behaves as a fixed-linear operator plus noise, irrespective of the input level. In the absence of an input, the injected noise can be treated as if it were a system input.

Because of display limits, the autopacer yields the score most nearly equal to the true limiting value when the system input is reduced and the excitation is due to operator remnant alone.

CR-674

## SECTION III

## MANIPULATOR EFFECTS

### A. PURPOSE

When mechanizing the autopaced critical tracking task, the experimenter must provide an appropriate control stick for the operator. Since different types of sticks have resulted in describing function differences in past experiments (ref. 13), it was expected that critical task scores would also reflect differences due to the manipulator. For this reason, an experiment was carried out to determine manipulator effects and, ultimately, to establish the suitability of the three commonly used types: pressure (isometric), spring restrained, and free (isotonic) sticks.

### B. THE EXPERIMENT

The experiment was carried out simultaneously with those of reference 1 and used the same measurement equipment and subject. Describing function and autopaced data were taken for the three types of control sticks available. The force stick, which was used for the bulk of the reference 1 experiments, was a Measurement Systems, Inc. No. 435 pencil stick approximately 9.2 cm (3-5/8 in.) long. It was mounted on an arm rest at the subject's right side and was used longitudinally (fore and aft) for compensatory tracking in the pitch axis. The free stick, consisting of a light aluminum rod attached to a low-torque potentiometer, was approximately 5.4 cm (2-1/8 in.) long and was mounted like the force stick. It had extremely small inertia and friction, which could not be detected by the operator. For the spring stick portion of the experiment, a spring was added to the free stick giving a gradient of 24.5 N/rad (1.54 oz/deg).

## C. RELEVANT NEUROMUSCULAR SYSTEM CHARACTERISTICS

Before discussing the data, a brief summary of a current neuromuscular model will be presented to orient the reader. It will be recalled from reference 1 that the effective time delay, $\tau_e$, is composed of three parts: the basic transport delay, equalization time constants, and neuromuscular system lags. The transport delay, $\tau_d$, includes nerve conduction times and computational time within the central nervous system, and is therefore invariant with control stick parameters. The lead and lag time constants, $T_L$ and $T_I$, are operator equalization parameters and are varied within limits as a function of the dynamic characteristics of the controlled element, and so are also invariant with the control stick. The neuromuscular system dynamics, then, are the only possible contributors to the effective time delay which can vary with manipulator, and will be discussed briefly here.

The dependence of the operator's phase lag (which determines the effective time delay) on the neuromuscular system can be seen by considering one current model (from ref. 14). A highly simplified block diagram is shown in figure 13. There, the system receives a command, $\alpha_c$, from the central nervous system and a limb position, $\delta$, results.

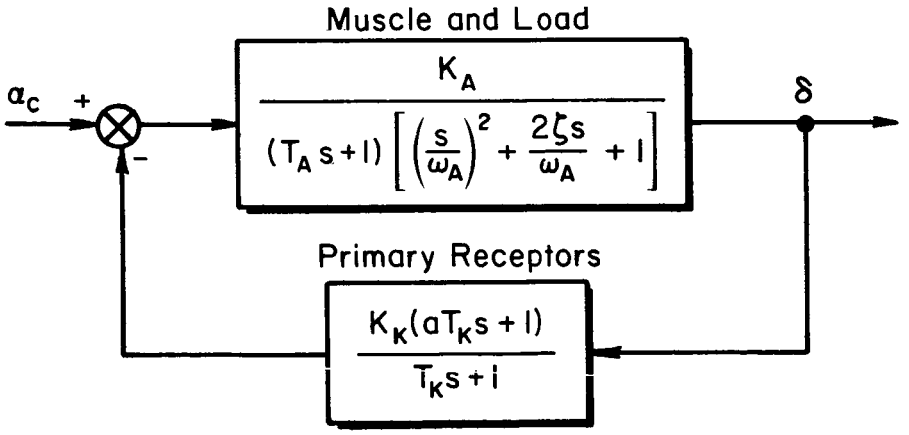


Figure 13. Block Diagram of Neuromuscular System

A high gain and a low gain loop closure of this system are both shown in figure 14a. The total open-loop Bode amplitude asymptotes are shown (solid line) along with segments of the open-loop $\sigma$-Bode, where, by substituting $s = -\sigma$ instead of $s = j\omega$ in the transfer function, the behavior of

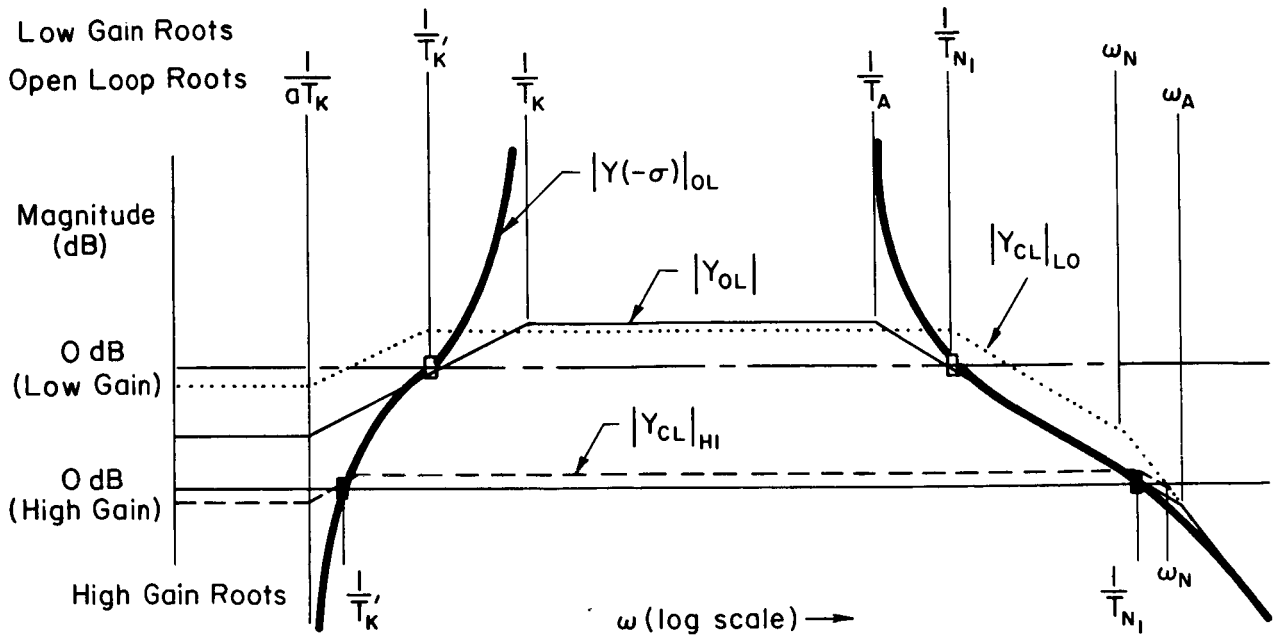


*a) Open Loop Bode Showing Closed Loop Roots*

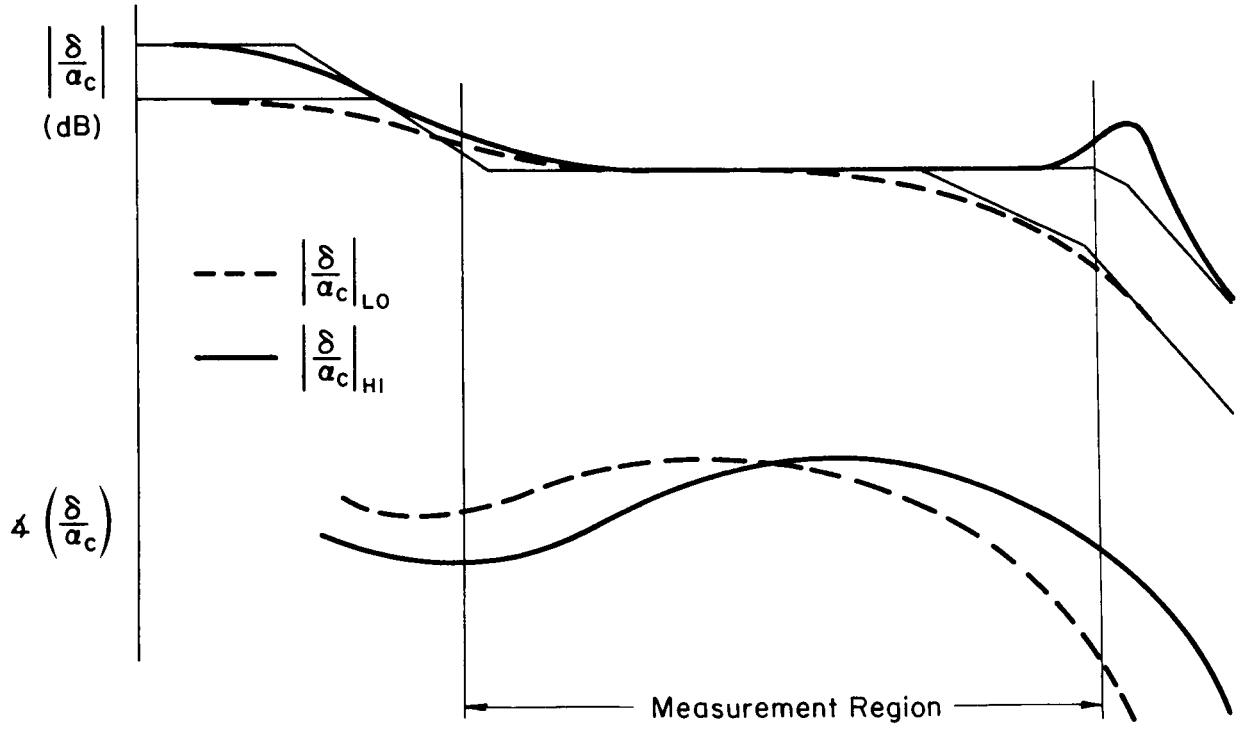


*b) Closed Loop Bode*

Figure 14. Neuromuscular System Bode Plots

closed-loop roots on the real axis can be easily determined (see ref. 8 for details). The closed-loop roots are found by constructing the closed-loop Bode, $Y_{CL} = GH/(1 + GH)$, which is shown by the dashed line. For contrast, a very low gain closure (dotted line) is also shown. Note the differences of the closed-loop roots, $1/T_K'$, $1/T_{N_1}$, and $\omega_N$, between the two closures.

Figure 14b shows the transfer function of interest, $\delta/\alpha_c$, obtained by dividing the feedback quantities out of the closed-loop plot of figure 14a $\left[\delta/\alpha_c = G/(1 + GH)\right]$. There the effects of the two gains are quite apparent, particularly in the phase. The increase in gain appears as a shift to the right of the phase curve. The measurement region shown in figure 14 spans approximately two decades.*

The contribution of the system of figure 14 to the operator dynamics is then

$$\frac{\delta}{\alpha_c} = \frac{K_A}{1 + K_A K_K} \frac{(T_K s + 1)}{(T_K' s + 1)(T_{N_1} s + 1)\left[\left(\frac{s}{\omega_N}\right)^2 + \frac{2\zeta_N s}{\omega_N} + 1\right]} \tag{6}$$

As noted in reference 1, the low frequency portion of the phase can be approximated by an exponential term, or

$$\angle \left(\frac{\delta}{\alpha_c}\right)_{low} \doteq \tan^{-1} T_K \omega - \tan^{-1} T_K' \omega \doteq \frac{1}{\omega}\left(\frac{1}{T_K'} - \frac{1}{T_K}\right) = -\frac{\alpha}{\omega} \tag{7}$$

Recalling that $e^{-j\alpha/\omega}$ is a special case of $e^{\alpha/s}$, the neuromuscular dynamics, which are commonly written in complex plane notation, are then approximately

$$\frac{\delta}{\alpha_c} \doteq \frac{K_N e^{\alpha/s}}{(T_{N_1} s + 1)\left[\left(\frac{s}{\omega_N}\right)^2 + \frac{2\zeta_N s}{\omega_N} + 1\right]} \tag{8}$$

*Practically, data to support the model at the low frequency end of the band is difficult to obtain accurately due to run length effects, which place theoretical limitations on the accuracy of any spectral analysis and which can be offset by an increased number of runs. The number of runs are limited in this experiment, consequently, the high frequency data will be the most reliable.

The effects of task difficulty and manipulator differences on the closed-loop model parameters can now be assessed. If the operator "tightens up" due to task difficulty by raising his gain, $K_A$, the phase curve will slide to the right with a resulting decreased $T_{N_1}$ and increased $\alpha$ and $\omega_N$. This "tightening up" phenomenon has been observed in other work (refs. 3 and 15) and was noted subjectively in the experiments of this program.

To assess manipulator effects, consider changing from a free stick to a force stick. The natural frequency, $\omega_A$, of the muscle and its load would be expected to increase as the inertia of the system decreased; consequently, an increase in the closed-loop root, $\omega_N$, would be expected. The extent to which the model describes the real situation of the critical task will be determined from the data.

## D. DESCRIBING FUNCTION DATA

The describing function data are shown in figure 15. Force and free stick data are shown together with spring stick data from reference 3 for a controlled element divergence of $\lambda = 2$ rad/sec. Also shown are data for the force and spring sticks for $\lambda = 4$ rad/sec (the spring stick of ref. 3 was laterally operated with a gradient of 35.2 N/rad, but in this experiment the longitudinal axis was used). A summary of the experimental variables appears in Table I.

Although the amplitude ratio can give some clues to behavior, the phase is of primary interest here because we are looking for effects on $\tau_e$. Before looking closely at the high frequency phase, some general observations can be made:

1. In the crossover region ($2 < \omega < 15$) the amplitude ratios for $\lambda = 2$ rad/sec are nearly coincident, as are those for $\lambda = 4$ rad/sec.
2. The usual increase in scatter is noticeable at the lower frequencies. The scatter generally averages out with a few runs, but here the available data is limited. Therefore, less emphasis can be placed on the low frequency data than would otherwise be desirable.
3. The high frequency phase shows surprisingly few differences due to the manipulator. This portion of the describing function will be scrutinized carefully after the data is curve fitted.

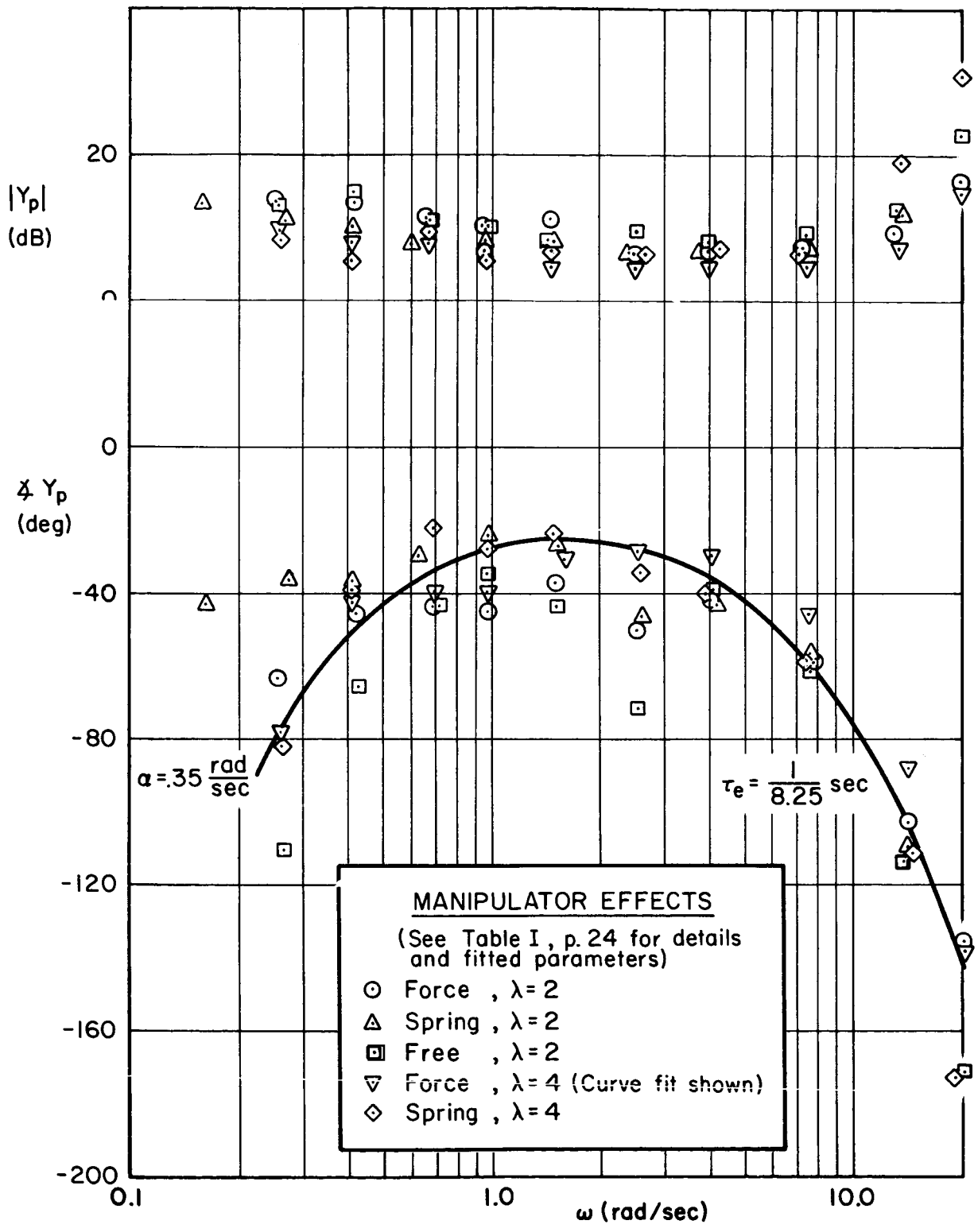


Figure 15. Describing Functions Showing Manipulator Effects

TABLE I

SUMMARY OF EXPERIMENTAL VARIABLES OF FIGURE 15

| SYMBOL | STICK TYPE | $\lambda$ (RAD/SEC) | INPUT | | | NO. OF RUNS | SUBJECT | SOURCE | $\alpha$ (RAD/SEC) | $\tau_e$ (SEC) | $1/\tau_e$ (RAD/SEC) |
|---|---|---|---|---|---|---|---|---|---|---|---|
| | | | SHAPE | $\omega_i$ (RAD/SEC) | $\sigma_i$ (IN.) | | | | | | |
| ⊙ | Force | 2 | B6' | 1.5 | 1/8 | 3 | JDM | This program | 0.35 | 0.121 | 8.25 |
| △ | Spring-Roll Tracking* | 2 | B6 | 1.5 | 1/2 | 8 | Four Different | Fig. 49 of Ref. 3 | 0.25 | 0.128 | 7.85 |
| ⊡ | Free | 2 | B6' | 1.5 | 1/8 | 2 | JDM | This program | 0.44 | 0.133 | 7.55 |
| ▽ | Force | 4 | B6' | 1.5 | 1/8 | 9 | JDM | Fig. 20 of Ref. 1 | 0.35 | 0.110 | 9.10 |
| ◇ | Spring | 4 | B6' | 1.5 | 1/8 | 2 | JDM | This program | 0.44 | 0.133 | 7.55 |

*All others—pitch tracking

The phase portion of the extended crossover model fits to the describing functions are shown in figure 15. The model is given by

$$Y_p = K_p e^{-j(\alpha/\omega + \tau_e \omega)} \qquad (9)$$

where the $\alpha$ accounts for the low frequency phase "droop" and the $\tau_e$ fits the high frequency lag. The $\tau_e$ is, by definition, the average effective time delay and is the parameter that the autopacer attempts to measure.

The rules for fitting are to fit the $\tau$ on the frequency points above crossover, which are considered to be highly reliable and repeatable points, and to fit the $\alpha$ on the points below the crossover frequency. The low frequency points are less reliable since there are fewer cycles in a computation period (run length). Past experience (ref. 3) has shown that several runs often need to be averaged before a stable $\alpha$ curve develops, so it is not surprising that low frequency scatter exists.

The results of the curve fits are given in table I (to avoid clutter in fig. 15, only the curve fit for the force stick with $\lambda = 2$ is shown). It is seen there that the force stick results in the minimum effective delay time, and that the $\tau_e$ obtained from the spring stick falls between the force and the free stick values. These observations are consistent with past data, reference 13, and autopaced data to be discussed next. It implies that the neuromuscular system tightens up with $\lambda$ and that its natural frequency increases as the manipulator is changed from a free stick to a force stick. The actual change, as exhibited in figure 15, is slight but is considered significant.

## B. AUTOPACED DATA

During the experimental series the subject made autopacer runs with the force, spring, and free sticks. The data are shown in figure 16. Each data point shown is an average of five trials. The lines connect comparable runs made on the same day. The total averages for the entire series with and without input are also shown. The differences between the daily runs and the total averages reflect the day-to-day variation in the five trial means.

The autopaced data shows the same trends with manipulator as did the describing function $\tau_e$, i.e., the $T_c = 1/\bar{\lambda}_c$ resulting from the force

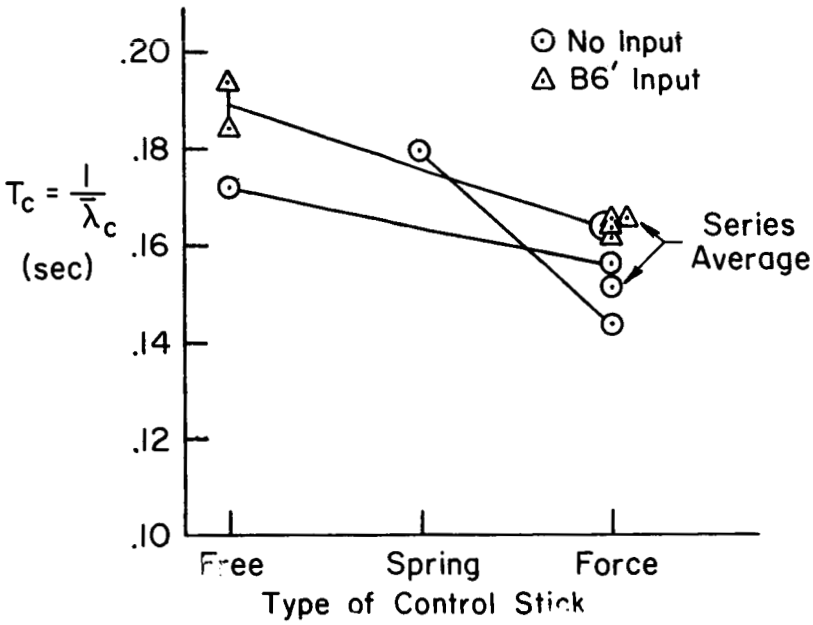


Figure 16. Autopacer Data for Three Types of Control Sticks

stick is about 90 percent of the free stick value. The spring stick autopaced data results in a rather large $T_c$. This anomaly cannot be resolved since only five trials were made with the spring stick. However, it is noted that the trend for that day was consistent with the other day's trends and also with the describing function trends.

A comparison of the fitted $\tau_e$'s (from Table I) from the describing functions and autopacer $T_c$'s obtained without an input is made directly in the regression diagram of figure 17. The $\tau_e = 0.75\ T_c$ line appears to be the best fit to the data.

## F. REMNANT DATA

The relative amount of power in the operator's output which is correlated with the input is called the relative remnant and is defined as

$$\rho_a = \sqrt{1 - \frac{\overline{n^2}}{\overline{c^2}}}$$

where

$n$ = uncorrelated signal in the operator's output

$c$ = total operator's output

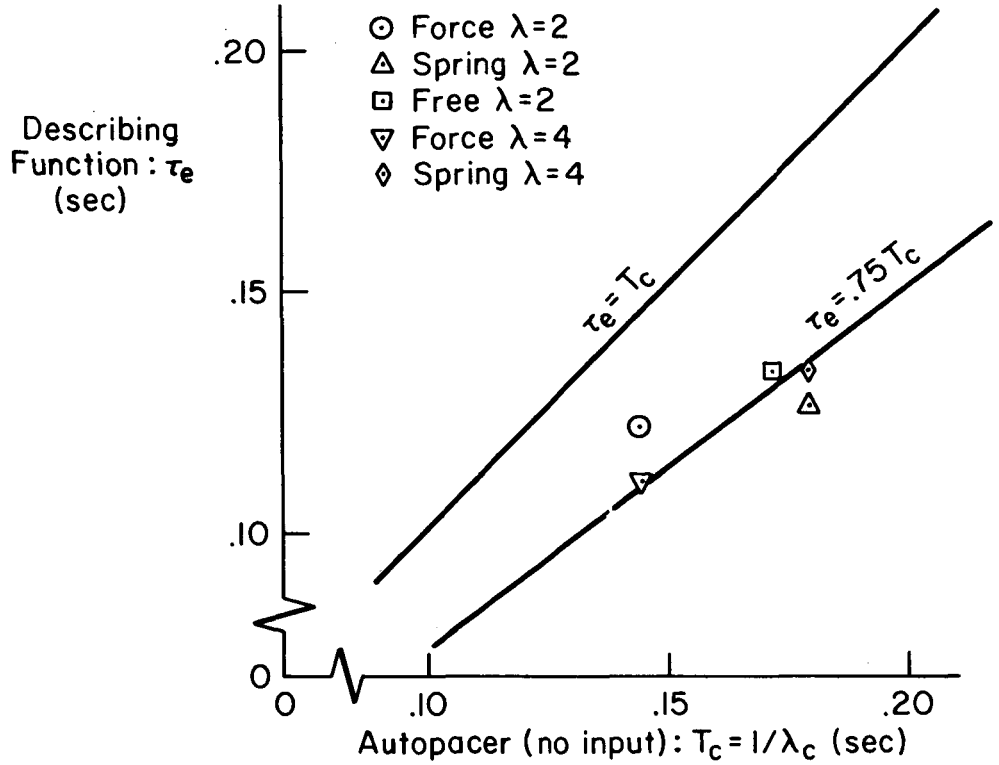


Figure 17. Regression Diagram for Describing Function Fitted $\tau_e$ and Autopacer $T_c$

The remnant was computed from available spectral analyzer data and is shown in figure 18 for the describing function runs of table I. The reference 3 spring stick remnant data for $\lambda = 2$ is averaged data of four operators. It does tie in satisfactorily, however, with the data of this experiment.

The remnant data shows that the operator becomes increasingly "noisy" when going from a force stick to a free stick. The reasons for this are not clear, but similar observations have been made elsewhere (ref. 13). It is most likely that both force level and displacement level influence remnant behavior to some extent.

## G. SUMMARY AND CONCLUSIONS

The describing function and autopacer data clearly indicate that the minimum effective time delay is exhibited by an operator using a force stick, while sticks requiring hand or finger displacement lower the natural frequencies of the stick-arm combination, causing an increase

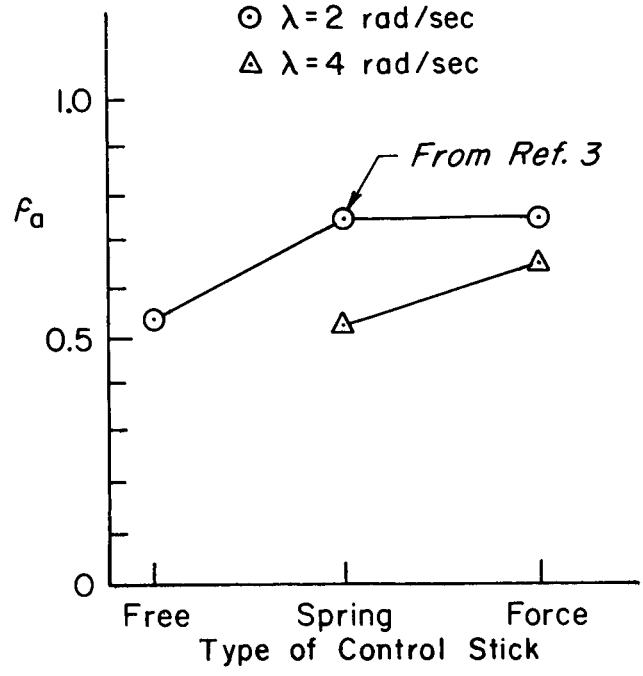


Figure 18. Relative Remnant for Three Types of Control Sticks

(only slight for the sticks tested) in the operator's effective time delay. The data further indicates, when considered with the remnant data, that there is no essential change in the operator's mode of behavior with manipulator. We can therefore draw conclusions about the two common applications and the results can be extrapolated to other situations as required by the experimenter.

One of the likeliest applications of the critical task is to measure the crucial parameter, $\tau_e$, of the operator that he would exhibit while tracking in a specific vehicle. The parameter then is a measure of the operator's capability and proficiency. Since stick differences are reflected in the measure, it should be made with a stick resembling as closely as possible the one in the actual tracking situation.

On the other hand, if the experimenter is attempting to determine the effects of stressors, environment, etc., on operator tracking behavior, performance, and characteristics, it is the perturbations about the base values that are of interest. The experimenter can therefore use the stick of his choice as long as he keeps in mind that the perturbation effects are not necessarily transferable between stick types.

# SECTION IV

# STEP REACTION TIME DATA AND TRIAL SIZE DETERMINATION

## A. STEP REACTION TIME DATA

### 1. General

The critical task measures the effective time delay of an operator, which is the continuous tracking analogy of the discrete measure step reaction time delay. Because of this analogy, it is of interest to directly compare the two measures since any correlation between them has never really been established. For this reason, some step reaction time measures were made; the resulting data and comparisons with effective time delay are given here.

### 2. The Experiment

The step reaction time data were taken during the experimental program when the describing function and autopaced runs were made at the Franklin Institute. A relay-controlled integrator was used to measure the time lapse between stimulus and response. The display and control stick were identical to those used in the tracking tasks, i.e., a horizontal bar on the CRT which displaced vertically, and a force stick was used. The subject was instructed to quickly return the bar to the crosshairs by applying pressure to the force stick when the bar unexpectedly displaced. Twenty responses were obtained per run, and the runs were integrated into the experimental plan so that they occurred adjacent to an autopaced run.

Two types of reaction time, RT, were measured: simple, where one polarity of stimulus was applied; and disjunctive, where the bar could displace in either direction. Both the direction of the displacement, when disjunctive RT was measured, and the foreperiod of the reaction (the time lapse between the warning signal and the stimulus, $0 < t_f < 5$ sec) were random.

## 3. Data

The data is shown in figure 19. The reciprocal of the run means rather than the means themselves are plotted for two reasons: (1) the reciprocal is directly comparable with the $\lambda$ scores (in rad/sec) obtained from the autopacer, and (2) there is evidence that 1/RT is normally distributed (ref. 9), which implies that nerve conduction velocity may have a Gaussian distribution about its mean. It can be noted in the figure that the deviation is considerable; the average ratio of standard deviation to mean is 21 percent. The ratio obtainable under the best of conditions is 10–13 percent (ref. 10, p. 38), so that the measures here are considered to be typical RT measures.

A comparison of step reaction time delay with either effective delay time or critical task score ($\lambda_c$) is a comparison of two different types of measures. The reaction time delay is a discrete measure with a very limited number of degrees of freedom (approximately equal to the number of trials), whereas the describing function and critical task measures are continuous measures and contain a considerably higher number of degrees of freedom (proportional to bandwidth times run length). We would therefore expect a higher variability in the step reaction time delay, which is indeed the case (the ratio of standard deviation to mean for the autopacer scores is approximately 6.5 percent for five trial samples).

Since the three kinds of measures were made at essentially the same psychological and physiological times, and with the same display and manipulator, a regression diagram could be drawn to indicate the connection, if any, between the measures. There would, however, be a degree of arbitrariness in "pairing off" the adjacent measures. The behavior of the sample means are therefore compared by normalizing them (dividing by the mean for the total experiment) and plotting them in the order of occurrence in figure 20. The elapsed time between each successive run of an "AM" or "PM" group is approximately 5 min.

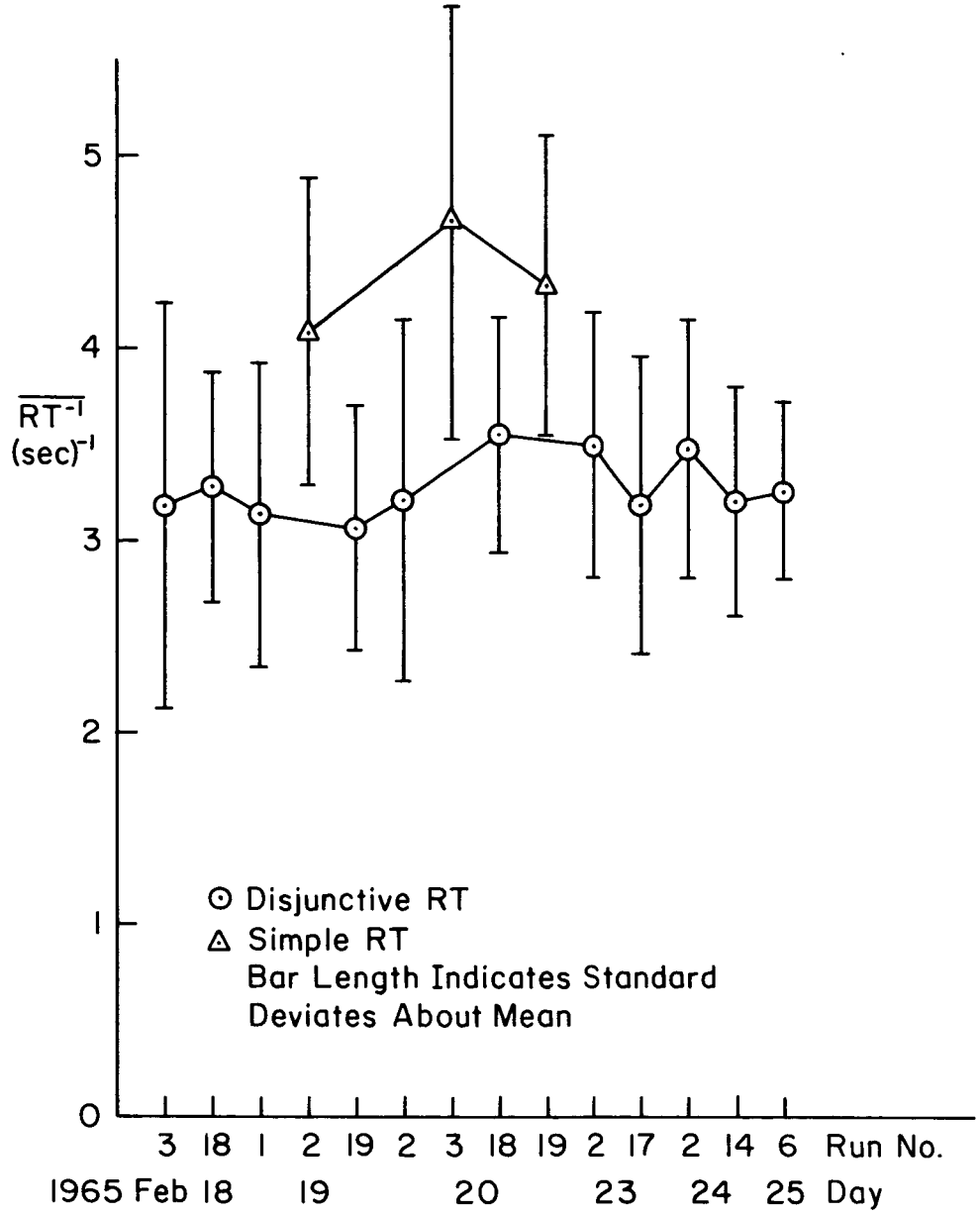


Figure 19. Run-to-Run Variability of the 20-Trial Reaction Time Samples

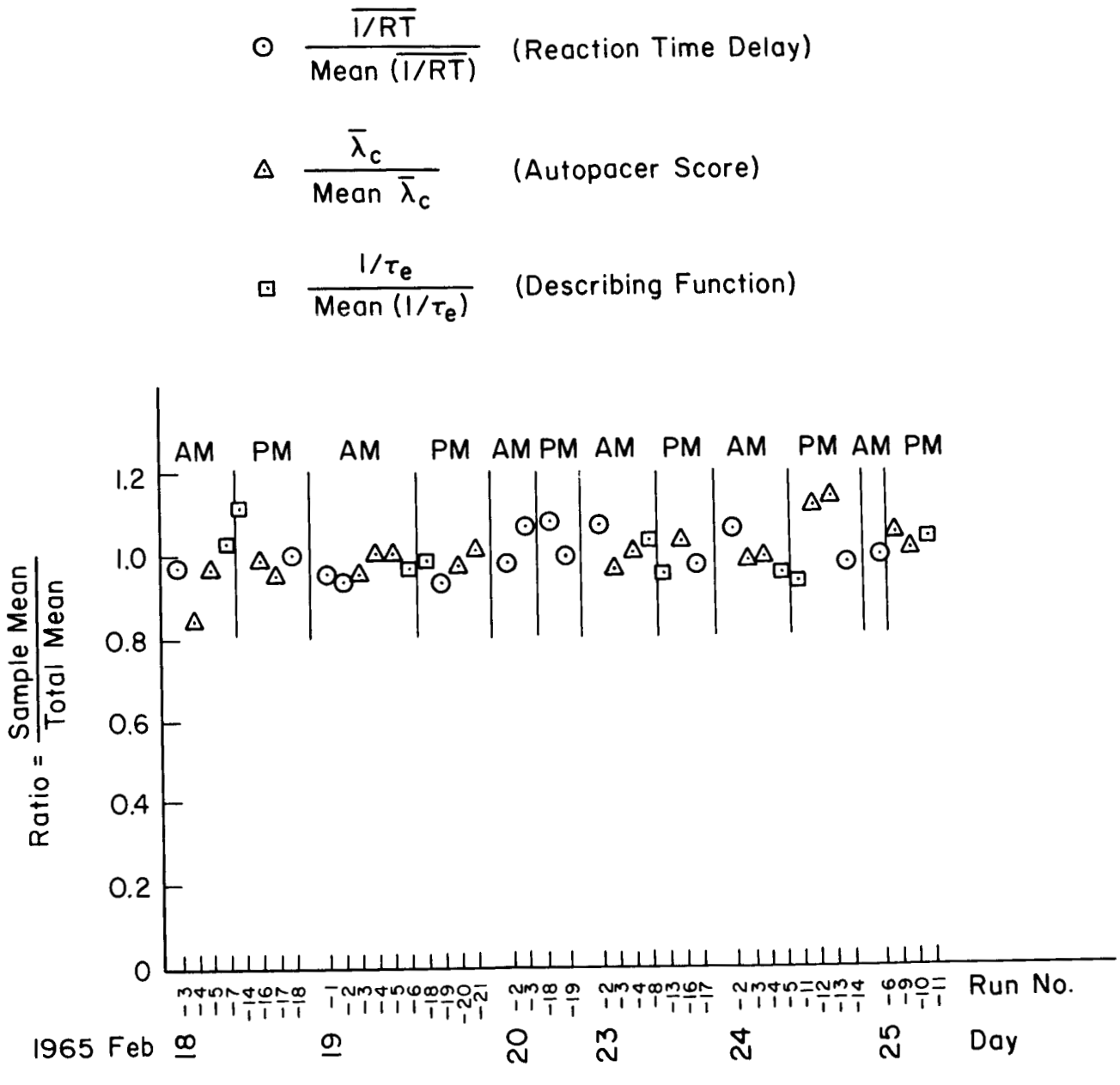


Figure 20. Temporal Trends of Normalized Sample Means for Three Types of Measures

The distribution in figure 20 has a random appearance, i.e., there is no noticeable correlation between the variations in the adjacent measures for this subject. The variations are due to random variables, then, and do not reflect a short term or steady-state change in the operator's characteristics.

### 4. Summary and Conclusions

Comparison of autopaced scores with step reaction time delay supports the conclusions of reference 1 that valid measures are obtainable with as few as five trials in a sample. The ratio of the deviations of the mean to the over-all mean is approximately 6.5 percent, which compares quite favorably with a 21 percent ratio for step reaction time delay for twenty trial samples.

A cursory look at the short term variations of the means indicate that they are random, i.e., an increase in an autopaced score sample does not imply a corresponding decrease in an immediately following step reaction time delay measure.

## B. DETERMINATION OF TRIAL SIZE

### 1. General

A primary use of the critical task is intended to be the determination of the effects of various environmental and stressor factors on critical task scores. Since some situations might be difficult to generate over long periods of time, a minimum number of trials to establish the effects should be predetermined. Here, a demonstrative example will be presented to show how such a determination might be made.

### 2. Analysis

It was shown in reference 1 that the critical task score, $\lambda_c$, exhibits a normal distribution about the mean for a single operator under what might be termed a "normal" environment and set of circumstances. There, for the input case, it was shown that the parameters of the distribution

are $\bar{\lambda}_{c_1} = 6.00$ rad/sec, $s_1 = 0.39$, $n_1 = 46$ trials. The subscript 1 has been added to show that the parameters are for "condition 1," or the normal condition. Now let us assume that a second experiment is to be run with the same operator under a different set of conditions. We wish to detect any change in the score parameters due to the new environment. The four distinct possible outcomes to the experiment are summarized in table II (a treatment of each case is given on p. 395 of ref. 11). We shall only consider one of these (outcome B of table II) in our sample calculation. The treatment of the other three cases are as equally straightforward (the F-test is used to determine differences in variances). Since data to the contrary is lacking, the assumption that the variances are equal for our example is not unreasonable, and it can be easily checked when two experimental environments are available.

TABLE II

POSSIBLE OUTCOMES OF TWO INDEPENDENT EXPERIMENTS

| OUTCOME | MEANS | VARIANCES |
|---|---|---|
| A | $\bar{\lambda}_{c_1} = \bar{\lambda}_{c_2}$ | $\sigma_1^2 = \sigma_2^2$ |
| B | $\bar{\lambda}_{c_1} \neq \bar{\lambda}_{c_2}$ | |
| C | $\bar{\lambda}_{c_1} = \bar{\lambda}_{c_2}$ | $\sigma_1^2 \neq \sigma_2^2$ |
| D | $\lambda_{c_1} \neq \bar{\lambda}_{c_2}$ | |

A simple t-test will be used to determine the minimum trial size in the second experiment. Given two sets of independent observations, form the sample statistic

$$t_c = \frac{\bar{\lambda}_1 - \bar{\lambda}_2}{s\sqrt{\frac{1}{n_1} + \frac{1}{n_2}}} \tag{10}$$

with $n_1 + n_2 - 2$ degrees of freedom (ref. 11). We will specify the minimum difference of means which we want to detect as $|\bar{\lambda}_1 - \bar{\lambda}_2| = 0.5$ rad/sec. This is an engineering judgment and may need to be revised as experience is gained with different environments. For this example, the sample statistic becomes

$$t_c = \frac{1.28}{\sqrt{0.0218 + \frac{1}{n_2}}} \tag{11}$$

which is plotted in figure 21.

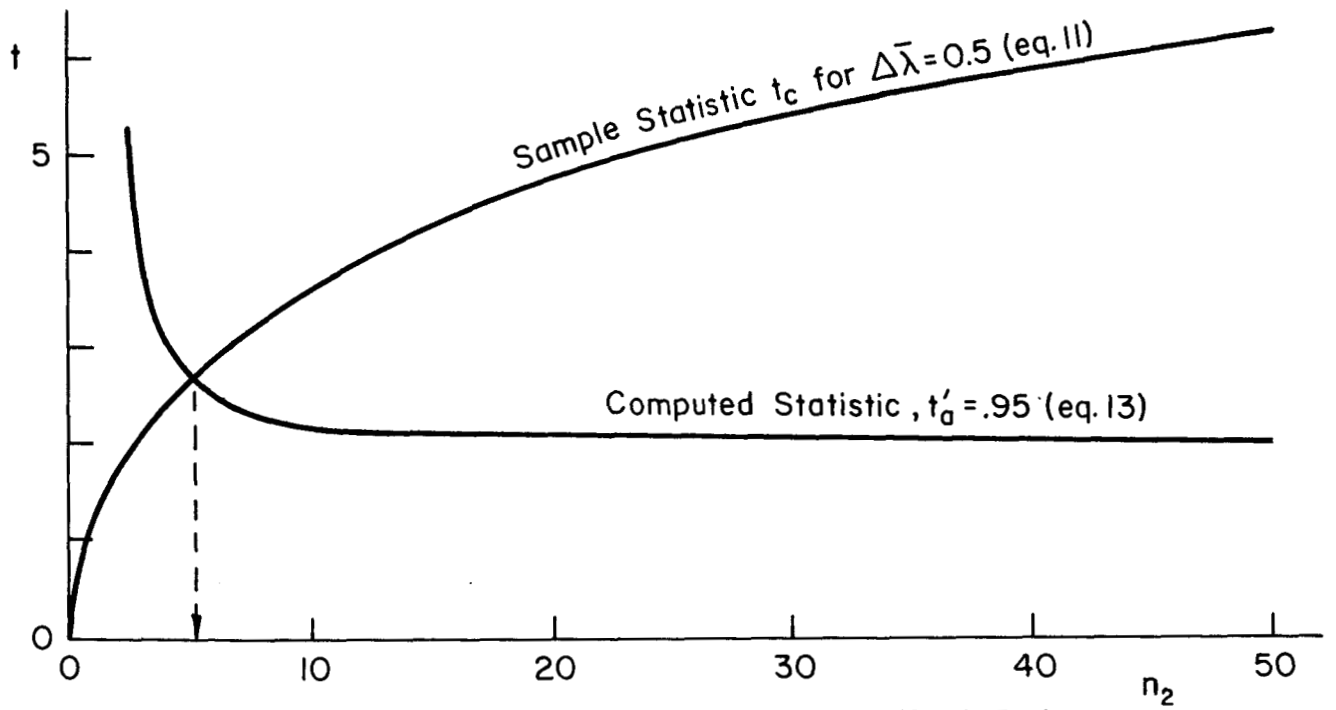


Figure 21. Trial Size Determination from the t-Test

The sample statistic, $t_c$, is to be compared with the computed statistic, $t'$, based on tables of the t-distribution. When the two experiments have different sample sizes, a modified form of $t'$ is appropriate. A reasonably conservative version (ref. 12) is

$$t' = \frac{\frac{s_1^2}{n_1} t_{a,n_1} + \frac{s_2^2}{n_2} t_{a,n_2}}{\frac{s_1^2}{n_1} + \frac{s_2^2}{n_2}} \tag{12}$$

where $t_{a,n}$ is the value found in the tables at the a-level of confidence for $n - 1$ degrees of freedom.

When $s_1 = s_2$, as is assumed above, equation (12) reduces to

$$t' = \frac{n_2 t_{a,n_1} + n_1 t_{a,n_2}}{n_1 + n_2} = \frac{2.015 n_2 + 46 t_2}{46 + n_2} \qquad (13)$$

for the example here. Equation (13) is plotted as a function of $n_2$ in figure 21 for a = 95% and $n_1 = 46$. The condition indicating a significant difference in means of 0.5 requires that

$$t' < t_c \qquad (14)$$

so it can be seen in the figure that at least six trials are needed. On the other hand, little is to be gained by running more than ten, so the experimenter would probably specify two samples of five trials each.

## 3. Conclusions

Having established a "base line" set of parameters for an operator under normal conditions, the experimenter can easily predict the number of trials necessary to detect a change of the mean under different conditions. The simplifying assumption, that variances remain unchanged, requires experimental verification, however, and should be among the first questions answered in future programs involving multiple test environments.

## SECTION V

## SECOND-ORDER TASK DATA

### A. GENERAL

During some of the initial analyses of the first-order critical task it became apparent that the addition of an integrator to the task would require the operator to generate large amounts of lead to stabilize the system. Such a second-order critical task might then measure not only the operator's time delay, as in the case of the first-order task, but might also provide an indication of the operator's lead generating capability. In order to obtain an appreciation of the magnitude of the problems involved in using the second task to yield useful and meaningful data, the experiment described below was carried out. The data obtained was rather meager, but nevertheless compares with that in reference 3 and expands the data base.

### B. THEORY

The second-order critical task is given by

$$Y_c = \frac{-K_c}{s(-Ts + 1)} \tag{15}$$

The form adopted by the operator, as shown in reference 3, can be described by the extended crossover model,

$$Y_p = K_p(T_L s + 1)e^{-j(\tau_e \omega + \alpha/\omega)} \tag{16}$$

where the operator attempts to cancel the integrator of the controlled element by using a large amount of lead, $T_L$. The total open-loop expression is thus

$$Y_p Y_c = \frac{K(T_L s + 1)}{s(-Ts + 1)} e^{-j(\tau_e \omega + \alpha/\omega)} \tag{17}$$

Generic root locus and Bode diagrams for the system are almost identical in appearance to figure 3 of reference 1, the exception being an extra pair of roots near the origin in the second-order root locus due to the lead term and integrator.

An exact analysis of the stability limits of the second-order task would require the solution of higher order equations, which cannot be done neatly in literal terms. However, a good approximate solution will be given here.

Appendix A of reference 1 gives for the first-order task at critical conditions:

$$\lambda_c \tau_e = 1 - \sqrt{\alpha \tau_e} \tag{18}$$

This result was obtained by first deriving an approximate expression for the phase in the crossover region (where the stability characteristics are determined) using the extended crossover model, then manipulating the phase equation to determine the stability limits. The total open-loop expression for the first-order task is

$$Y_p Y_c = \frac{K e^{-j(\tau_e \omega + \alpha/\omega)}}{-Ts + 1} \tag{19}$$

where $\lambda \equiv 1/T$.

Comparison of equations (17) and (19) indicates that the difference between the phases of the two tasks is given by

$$\Delta\varphi_L = \angle \frac{(T_L s + 1)}{s} = -\frac{\pi}{2} + \tan^{-1} T_L \omega \tag{20}$$

which can be approximated in the crossover region, where $T_L \omega \gg 1$, as

$$\begin{aligned} \Delta\varphi_L &\doteq -\frac{\pi}{2} + \frac{\pi}{2} - \frac{1}{T_L \omega} \\ &\doteq -\frac{1}{T_L \omega} \end{aligned} \tag{21}$$

Note that this contribution to the phase is of the same form as the $\alpha$ term in equation (19). The effect of $T_L$ on $\lambda$ is thus obtained simply by replacing the $\alpha$ of equation (18) by $\alpha + 1/T_L$, resulting in

$$\lambda_c \tau_e = 1 - \sqrt{(\alpha + 1/T_L)\tau_e} \qquad (22)$$

Thus, the differences between the theoretically obtainable scores for the first- and second-order critical tasks are clearly shown by a comparison of equations (18) and (22). The total effect of requiring the operator to greatly increase his lead is to reduce $\lambda_c$ for two reasons. First, the effective time delay, $\tau_e$, is increased since high frequency lead is no longer available to help cancel out high frequency neuromuscular system lags. Second, the phase margin is reduced slightly because of the increased low frequency phase "droop" (i.e., an increase in the apparent $\alpha$).

The data taken to validate this theoretical effect is given next.

## C. DESCRIBING FUNCTION DATA

Describing functions were measured for two values of $\lambda$. Two runs were made for $\lambda$ = 1 rad/sec, which was moderately difficult to control for four minutes, and five runs were made for $\lambda$ = 2 rad/sec, which was nearly at the operator's controllability limit. The B6' – 1.5 – 1/8 in. input was used in all runs.

The resulting describing functions are shown in figures 22 and 23. Also shown in the figures are the extended crossover model fits. The figures are very similar in general appearance, specifically:

- Large low frequency phase variation is present, due to a small number of runs and/or large variability in lead generation.
- A high frequency phase droop at a considerably higher rate than that provided by the model. This condition would be improved by fitting with a precision model, where the neuromuscular system dynamics give a more rapidly lagging phase with

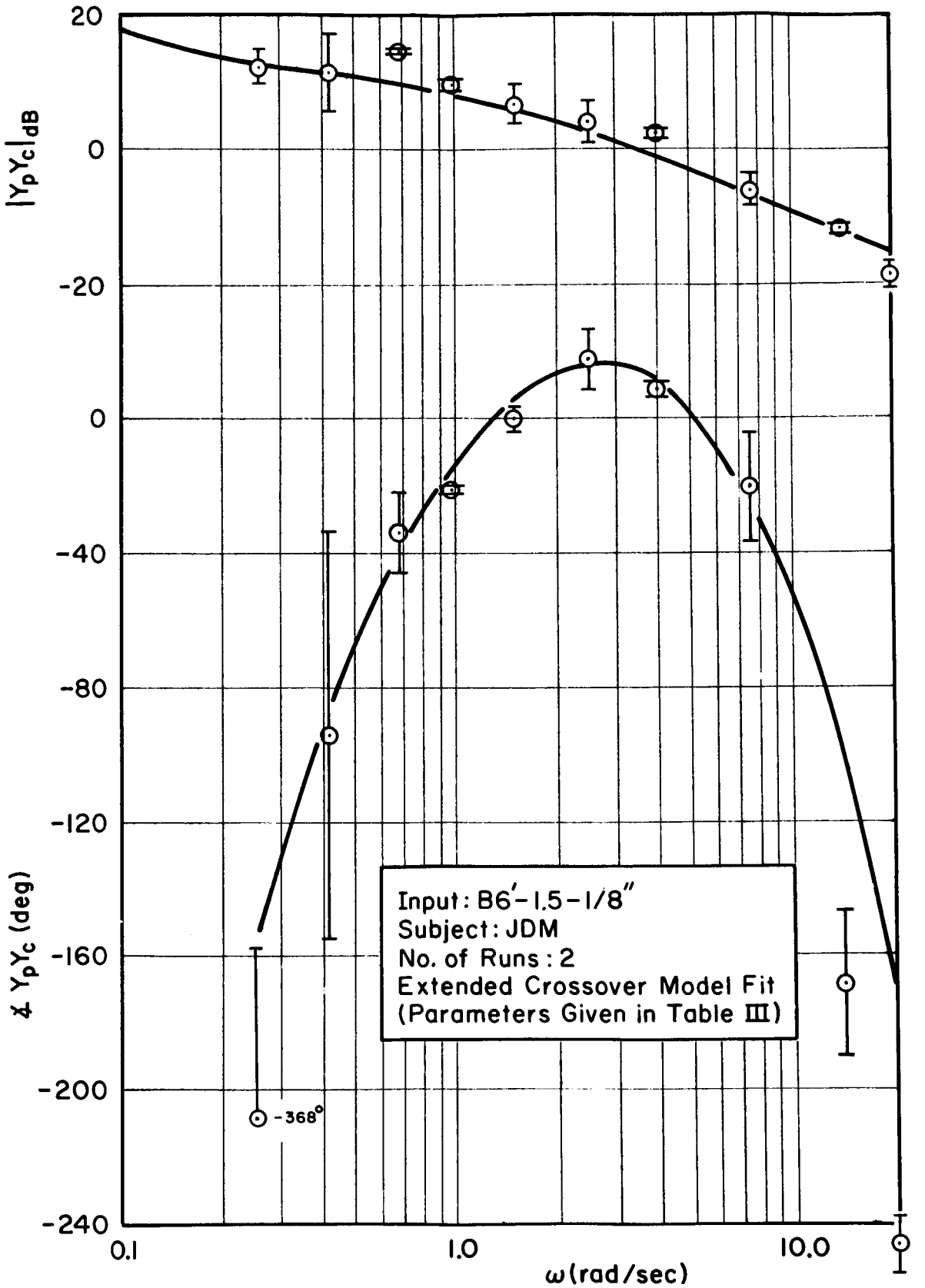


Figure 22. Measured Describing Functions, $Y_c = 5/s(s - 1)$

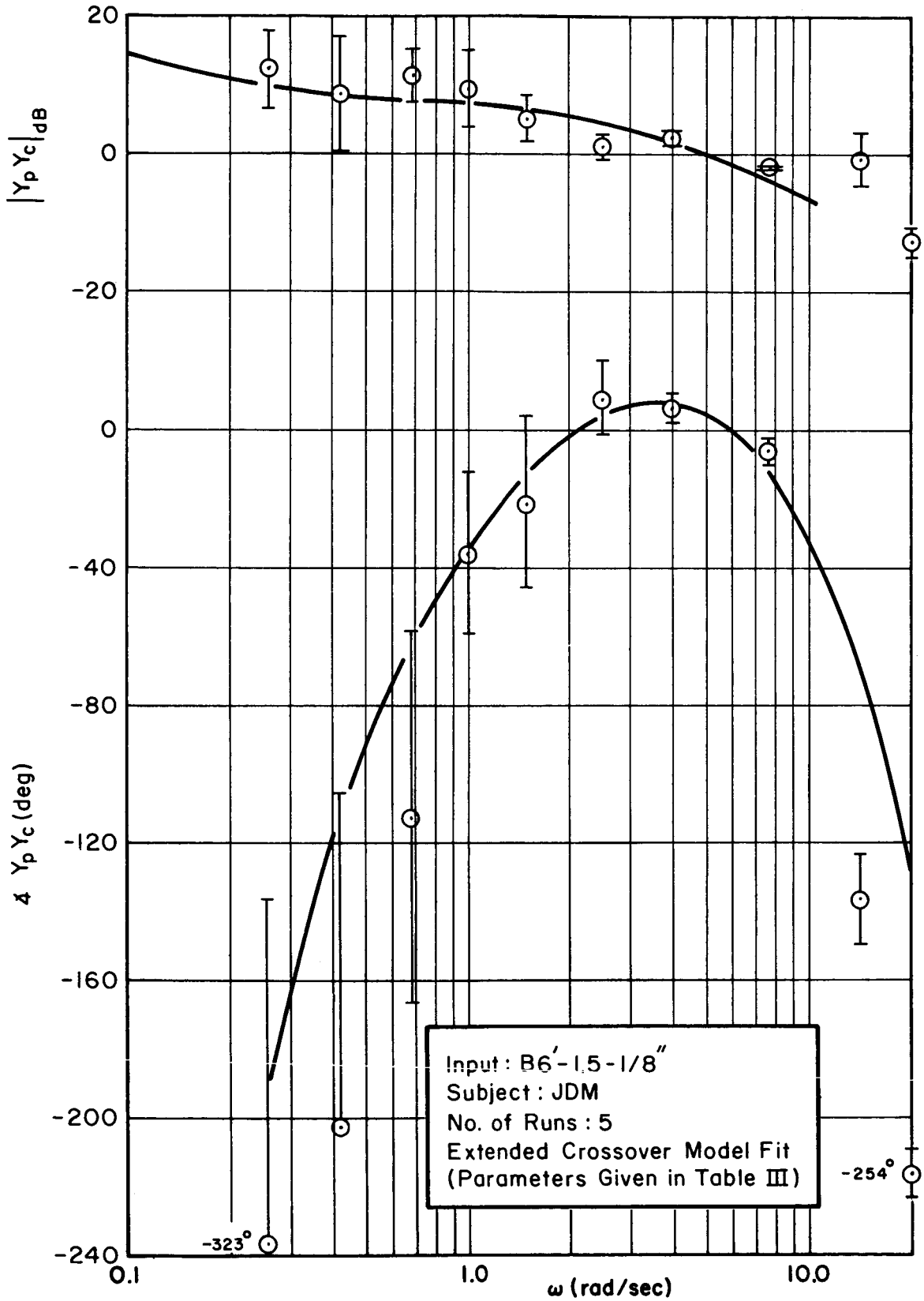


Figure 23. Measured Describing Functions, $Y_c = 10/s(s - 2)$

frequency. Since both models are the same in the crossover region and since the data are not as numerous as might be desired, the precision model fit will not be made.

- Low phase margins (on the order of 10 deg) are demonstrated, indicating the difficulty of the task.

A difference of note between the two cases is the high frequency amplitude ratio for the $\lambda = 2$ case. There the peak due to the neuromuscular second-order pair is obvious. Here again, the precision model would improve the fit greatly.

A comparison of the $\alpha$-model fitting parameters is shown in table III, together with the parameters of the second-order task data of reference 3. The effective time delay shows a decrease with increasing task difficulty, as it did in the first-order case. There is also a fairly large increase in $\alpha$, which is presently unexplained. The relative remnant, $\rho_a$, indicates

TABLE III

COMPARISON OF SECOND-ORDER FITTED PARAMETERS

| CONTROLLED ELEMENT | $Y_c = \frac{K_c}{s(s-1)}$ | | $Y_c = \frac{K_c}{s(s-2)}$ |
|---|---|---|---|
| | TABLE XIII REF. 3 | PRESENT EXPERIMENT | PRESENT EXPERIMENT |
| Input | B6'-1.5-1/4 in. | B6'-1.5-1/8 in. | B6'-1.5-1/8 in. |
| No. of Runs | 12 | 2 | 5 |
| $\omega_c$ (rad/sec) | 3.7 | 3.5 | 5.2 |
| $\varphi_M$ (deg) | 7.0 | 15.0 | 5.0 |
| $\tau_e$ (sec) | 0.31 | 0.23 | 0.19 |
| $\alpha$ (rad/sec) | 0.37 | 0.57 | 0.70 |
| $\alpha\tau_e$ | 0.12 | 0.13 | 0.13 |
| $\omega_{u1}$ (rad/sec) | 1.2 | 1.3 | 2.1 |
| $\omega_{u2}$ (rad/sec) | 3.7 | 5.22 | 6.0 |
| $1/T_L$ (rad/sec) | 0.20 | 0.20 | 0.20 |
| $K_p\left(\frac{cm}{cm/sec^2}\right)$ | 3.8 | 3.6 | 2.5 |
| $\rho_a$ | 0.47* | 0.69 | 0.49 |

*Average for five subjects. Range: $0.21 < \rho_a < 0.56$

that the over-all signal to noise ratio is lower than in the first-order case, and so decreases with task difficulty ($\rho_a$ = 0.49 vs about 0.7) which further supports the existence of the low frequency scatter.

The limited data with its attendant scatter leaves some arbitrariness in the low frequency fitting of $\alpha$ and $1/T_L$; consequently, further speculation on the cause and effect relationship for this data will be curtailed. Nevertheless, the describing function results can be compared with the autopacer data to follow.

## D. AUTOPACER DATA

During the experimental program, a limited amount of second-order autopaced data were taken to find the effects of lead generation on $\lambda_c$. Three samples of five trials each were made with an input, and a like number were made without an input. These data are plotted in figure 24 where the five trial means are shown by the symbols with the standard deviations shown by the bars. The ratio of deviation to mean is 10 percent for the B6' input case and 11 percent with no input. This is approximately twice the ratio observed for the first-order data, but still compares quite favorably with the 21 percent ratio observed for the step reaction time data (see Section IV-A).

In Section V-B a theoretical relation for the autopacer score was derived (eq. 22) using the extended crossover model. The theory and data can now be compared. Using the values of $\tau_e$, $\alpha$, and $T_L$ from table III for the $\lambda_c = 2$ case, equation (22) yields

$$\lambda_{c_{DF}} = \frac{1}{0.185}\left(1 - \sqrt{(0.70 + 0.20)\ 0.185}\right) \tag{23}$$

$$\lambda_{c_{DF}} = 3.2 \text{ rad/sec}$$

This computed score is to be compared with the average autopacer limit of $\lambda_c$ = 3.2 rad/sec from figure 24. The remarkable agreement here raises an interesting question. Why is the operator able to track at such a

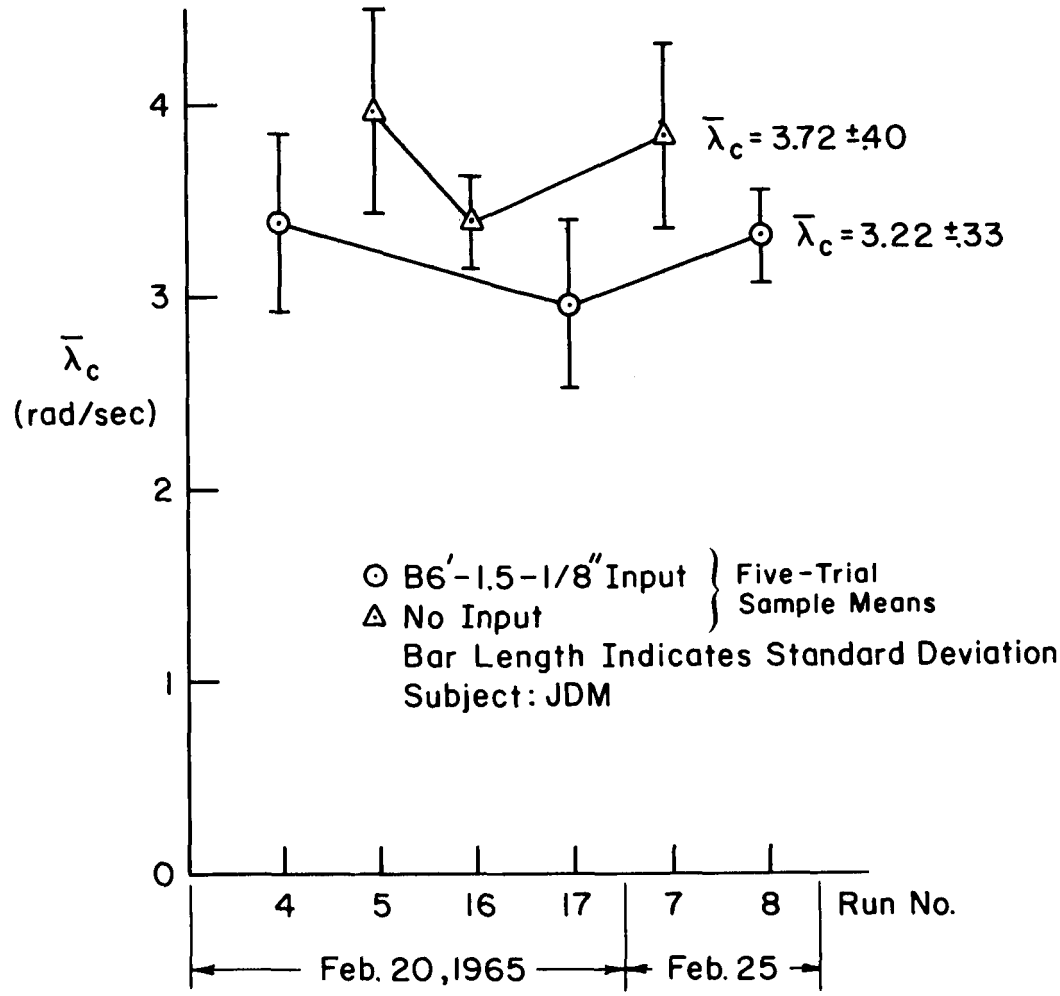


Figure 24. Second-Order Autopaced Data

small phase margin in the second-order case (5 deg here vs 12 deg for the first-order case, resulting in the accurate prediction of eq. 22) even though more variability in the data, and therefore in the operator was observed? In the first order results in reference 1 an 18 percent difference between predicted and observed scores was exhibited because the remnant was not included in the analysis.

Another unresolved observation regards the control stick. In the first-order case, the type of stick (force, spring, or free) made little difference in behavior (see Section III). For the second-order case, however, the operator was unable to control even the smallest instability

with the free stick. His subjective impression was that lack of a null-control reference was the difficulty. This difference between the first- and second-order free-stick critical tasks will hopefully be explained by one of the comprehensive neuromuscular system theories currently being developed.

## E. CONCLUSIONS

The operator behaves as predicted when tracking the second-order critical task. A remarkable, perhaps fortuitously good, agreement between the theoretical limit implied by the describing function data and the auto-paced limits was noted. The adjustment rules of the operator, however, are not clear, and will have to be the subject of future work. Because of this, and because of the relatively scant amount of second-order data available, it is concluded that the second-order critical task requires additional research before it can become as useful a tool as the first-order task.

## REFERENCES


1. Jex, H. R.; McDonnell, J. D.; and Phatak, A. V.: A "Critical" Tracking Task for Man-Machine Research Related to the Operator's Effective Delay Time. NASA CR-616, Oct. 1966.

2. McRuer, D. T.; and Krendel, E. S.: Dynamic Response of Human Operators. (WADC-TR-56-524, ASTIA AD-110693), Control Specialists, Inc., and Franklin Institute Laboratories for Research and Development, Oct. 1957.

3. McRuer, D.; Graham, D.; Krendel, E.; and Reisener, W., Jr.: Human Pilot Dynamics in Compensatory Systems—Theory, Models, and Experiments with Controlled Element and Forcing Function Variations. Tech. Rep. 115-1 (AFFDL-TR-65-15, DDC No. AD 470337), Systems Technology, Inc., Jan. 1965.

4. Elkind, J. E.: Characteristics of Simple Manual Control Systems. Tech. Rep. 111, Lincoln Lab., Mass. Inst. of Tech., Apr. 1956.

5. Seltzer, L. J.; and D. T. McRuer: Survey of Analog Cross Spectral Analyzers. (WADC-TR-59-241), Systems Technology, Inc., Dec. 1959.

6. Durand, T. S.: Some Preliminary Experiments on the Critical Task for Reaction Time of a Tracking Operator. Working Paper 147-1, Systems Technology, Inc., 25 Aug. 1964.

7. Phatak, A. V.: Theoretical Performance and Stability of a Single First-Order Critical Task. Working Paper 147-3, Systems Technology, Inc., Jan. 1965.

8. McRuer, Duane T.: Unified Analysis of Linear Feedback Systems. Tech. Rep. 14 (ASD-TR-61-118, DDC No. AD 270593), Systems Technology, Inc., July 1961.

9. Tsibulevskii, I. E.: Operator Delay in Processing Visual Signals. Automatika i Telemekhanika, vol. 23, no. 11, Nov. 1962, pp. 1513—1526.

10. Woodworth, Robert S.; and Harold Schlosbert: Experimental Psychology. Ref. ed., Holt, Rinehart and Winston, 1964.

11. Hald, A.: Statistical Theory with Engineering Applications. John Wiley and Sons, New York, 1952.

12. Cochran, W. G.; and Cox, G. M.: Experimental Designs. Second ed., John Wiley and Sons, New York, 1957.

13. McRuer, D. T.; and Magdaleno, R. E.: Human Pilot Dynamics with Various Manipulators. Tech. Rep. 134-3, Systems Technology, Inc., July 1966.

14. Magdaleno, R. E.: Neuromuscular Subsystem—Data and Models. Working Paper 154-1, Systems Technology, Inc., 8 Oct. 1965.

15. Okabe, Y.; Rhodes, H. E.; Stark, L.; and Willis, P. A.: Transient Responses of Human Motor Coordination System. QPR 66, Res. Lab. Elec., Mass. Inst. of Tech., July 1962, pp. 389—395.



NASA-Langley, 1967

*"The aeronautical and space activities of the United States shall be conducted so as to contribute . . . to the expansion of human knowledge of phenomena in the atmosphere and space. The Administration shall provide for the widest practicable and appropriate dissemination of information concerning its activities and the results thereof."*

—NATIONAL AERONAUTICS AND SPACE ACT OF 1958

# NASA SCIENTIFIC AND TECHNICAL PUBLICATIONS

**TECHNICAL REPORTS:** Scientific and technical information considered important, complete, and a lasting contribution to existing knowledge.

**TECHNICAL NOTES:** Information less broad in scope but nevertheless of importance as a contribution to existing knowledge.

**TECHNICAL MEMORANDUMS:** Information receiving limited distribution because of preliminary data, security classification, or other reasons.

**CONTRACTOR REPORTS:** Technical information generated in connection with a NASA contract or grant and released under NASA auspices.

**TECHNICAL TRANSLATIONS:** Information published in a foreign language considered to merit NASA distribution in English.

**TECHNICAL REPRINTS:** Information derived from NASA activities and initially published in the form of journal articles.

**SPECIAL PUBLICATIONS:** Information derived from or of value to NASA activities but not necessarily reporting the results of individual NASA-programmed scientific efforts. Publications include conference proceedings, monographs, data compilations, handbooks, sourcebooks, and special bibliographies.

*Details on the availability of these publications may be obtained from:*

SCIENTIFIC AND TECHNICAL INFORMATION DIVISION

NATIONAL AERONAUTICS AND SPACE ADMINISTRATION

Washington, D.C. 20546